WRDC-TR-89-4089

ULTRA HIGH TEMPERATURE CERAMIC-CERAMIC COMPOSITES

Professor K. Vedula
Case Western Reserve University
Cleveland, Ohio 44106

October 1989

Final Report for Period October 1986 - April 1989

Approved for public release; distribution unlimited

MATERIALS LABORATORY
WRIGHT RESEARCH AND DEVELOPMENT CENTER
AIR FORCE SYSTEMS COMMAND
WRIGHT-PATTERSON AIR FORCE BASE, OHIO 45433-6533

NOTICE

When Government drawings, specifications, or other data are used for any purpose other than in connection with a definitely government-related procurement, the United States Government incurs no responsibility or any obligation whatsoever. The fact that the government may have formulated or in any way supplied the said drawings, specifications, or other data, is not to be regarded by implication, or otherwise in any manner construed, as licensing the holder, or any other person or corporation; or as conveying any rights or permission to manufacture, use, or sell any patented invention that may in any way be related thereto.

This report is releasable to the National Technical Information Service (NTIS). At NTIS, it will be available to the general public, including foreign nations.

This technical report has been reviewed and is approved for publication.

LAWRENCE E. MATSON
Project Engineer
Processing and High Temperature
Materials Branch
Metals and Ceramics Division
FOR THE COMMANDER

ALLAN P. KATZ
Technical Area Manager
Processing and High Temperature
Materials Branch
Metals and Ceramics Division

NORMAN M. GEYER, Acting Chief
Processing and High Temperature
Materials Branch
Metals and Ceramics Division

If your address has changed, if you wish to be removed from our mailing list, or if the addressee is no longer employed by your organization, please notify WRDC/MLLM, WPAFB, OH 45433-6533 to help us maintain a current mailing list.

Copies of this report should not be returned unless return is required by security considerations, contractural obligations, or notice on a specific document.

Unclassified
SECURITY CLASSIFICATION OF THIS PAGE

REPORT DOCUMENTATION PAGE

Form Approved
OMB No 0704-0188

1a REPORT SECURITY CLASSIFICATION Unclassified	1b RESTRICTIVE MARKINGS
2a SECURITY CLASSIFICATION AUTHORITY	3 DISTRIBUTION/AVAILABILITY OF REPORT Approved for public release; distribution is unlimited
2b DECLASSIFICATION/DOWNGRADING SCHEDULE	
4 PERFORMING ORGANIZATION REPORT NUMBER(S)	5 MONITORING ORGANIZATION REPORT NUMBER(S) WRDC-TR-89-4089
6a NAME OF PERFORMING ORGANIZATION Case Western Reserve University 6b OFFICE SYMBOL (If applicable)	7a NAME OF MONITORING ORGANIZATION Wright Research and Development Center Materials Laboratory AFSC
6c ADDRESS (City, State, and ZIP Code) Cleveland, OH 44106	7b ADDRESS (City, State, and ZIP Code) WRDC/MLLM Wright-Patterson AFB, OH 45433-6533
8a NAME OF FUNDING/SPONSORING ORGANIZATION 8b OFFICE SYMBOL (If applicable)	9 PROCUREMENT INSTRUMENT IDENTIFICATION NUMBER F33615-86-C5118
8c ADDRESS (City, State, and ZIP Code)	10 SOURCE OF FUNDING NUMBERS PROGRAM ELEMENT NO: 62102F; PROJECT NO: 2420; TASK NO: 01; WORK UNIT ACCESSION NO: 86

11 TITLE (Include Security Classification)
Ultra High Temperature Ceramic-Ceramic Composites

12 PERSONAL AUTHOR(S)
Vedula, Krishna M.

13a TYPE OF REPORT	13b TIME COVERED	14 DATE OF REPORT (Year, Month, Day)	15 PAGE COUNT
Final	FROM Oct. 86 TO Apr. 89	October 1989	73

16 SUPPLEMENTARY NOTATION

17 COSATI CODES			18 SUBJECT TERMS (Continue on reverse if necessary and identify by block number)
FIELD	GROUP	SUB-GROUP	
1102			High Temperature Composites, Material Compatibility
1104			

19 ABSTRACT (Continue on reverse if necessary and identify by block number)

The focus of this project is an understanding of the material stability and environmental degradation of potential diboride reinforced oxide matrix composites exposed to oxidizing conditions at ultrahigh temperature in the range of 1650-2100°C.

Particulate composites of 5w%TiB_2 and 5w%ZrB_2 in YS-ZrO_2, Y_2O_3 and Al_2O_3, as well as of 5w%TiB_2 in $CaZrO_3$, have been prepared by vacuum hot pressing. Specimens were tested in vacuum at 1600°C, by induction heating in air at 1400 to 1850°C and oxyacetylene flames at 1650 to 2050°C, in order to evaluate the chemical compatibility between the diboride/oxide combinations, as well as the effectiveness of the oxides as diffusion barriers for the oxidation of the diborides.

Results indicate that, although the oxides and diborides are chemically compatible at these temperatures, the oxides are not effective in preventing the oxidation of the diborides.

20 DISTRIBUTION/AVAILABILITY OF ABSTRACT	21 ABSTRACT SECURITY CLASSIFICATION
☒ UNCLASSIFIED/UNLIMITED ☐ SAME AS RPT ☐ DTIC USERS	Unclassified
22a NAME OF RESPONSIBLE INDIVIDUAL Lawrence E. Matson	22b TELEPHONE (Include Area Code) (513) 255-9842 / 22c OFFICE SYMBOL WRDC/MLLM

DD Form 1473, JUN 86 *Previous editions are obsolete*

SECURITY CLASSIFICATION OF THIS PAGE
Unclassified

Continuation of Block 19

The oxide matrix composites oxidize very severely, particularly in the case of ZrO_2 and Y_2O_3. The large vapor pressure of B_2O_3 formed at the diboride/oxide interface presents serious problems in a very short period of time, when the composites are exposed to oxidizing conditions above 1600°C. Matrices of Al_2O_3 and $CaZrO_3$ are also not very effective, but are significantly better than ZrO_2 and Y_2O_3.

Since the oxides were not very effective, the ability of $MoSi_2$ to protect TiB_2 against oxidation at ultrahigh temperatures was studied using a particulate composite of 20w%TiB_2 in a matrix of $MoSi_2$. When heat treated in air at 1650°C, this composite forms a protective layer of borosilicate glass containing TiO_2 whiskers. Although this layer is not as protective as pure silica which forms on the surface of the monolithic $MoSi_2$, the silicide matrix is far superior to the oxide matrices in protecting the diborides against oxidation.

Hence, although oxide matrices do not hold any promise for protecting diboride reinforcements in oxidizing conditions at these ultrahigh temperatures, it may be possible to use silicides as either a matrix or as a diffusion barrier to protect diborides against oxidation.

PREFACE

This report is based on the assistance of several graduate students, including Ahmed Abada, Fred Lisy, Joseph Rigney and Joseph Wang. The financial support of Wright-Patterson Air Force Base, through their Ultrahigh Temperature Ceramic-Ceramic Composites initiative is gratefully acknowledged.

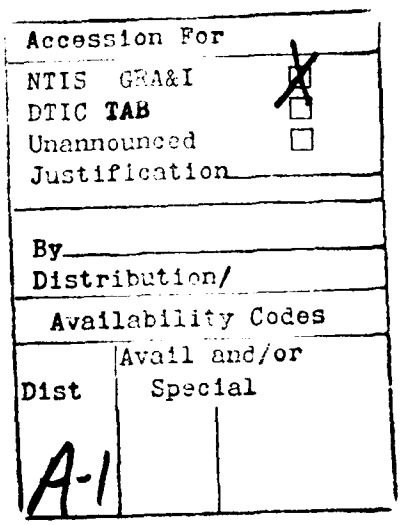

CONTENTS

LIST OF FIGURES

LIST OF FIGURES (Continued)

LIST OF FIGURES (Continued)

LIST OF TABLES

1. INTRODUCTION

The focus of this project is an understanding of the material stability and environmental degradation of potential diboride reinforced oxide matrix composites exposed to oxidizing conditions at ultrahigh temperatures in the range of 1650-2100°C.

The specific diborides of interest are TiB_2 and ZrB_2, because of their high melting points and their superior strengths at the ultrahigh temperatures of interest.[1] The major emphasis of this project was on TiB_2 which is attractive because of its high melting point (2970°C), strength at very high temperatures and low density (4.52 g/cc). Figure 1 illustrates the phase diagrams for TiB_2 and ZrB_2, whereas Figure 2 compares the high temperature strength of TiB_2 with several other potential high temperature structural materials.

Although the diborides are attractive from the high temperature strength considerations, their major drawback is their susceptibility to oxidation. Hence, the critical aspects of the oxidation of diborides are reviewed in section 1.1.

The potential for using diborides as reinforcements in oxide matrices is of primary interest in this program. The matrix materials considered are ZrO_2 and Y_2O_3, because of their relatively high melting points (ZrO_2:2715°C, Y_2O_3:2410°C). In order for these oxide matrices to be effective in preventing oxidation of the diboride reinforcements, it is important to understand the kinetics of transport of oxygen through these oxides and this is summarized in section 1.2.

The potential for using silicides as additions to improve the oxidation resistance of diborides is another area of interest in this program. $MoSi_2$ has excellent high temperature oxidation resistance through the formation of a protective silica layer and is, hence, attractive as an addition or as a

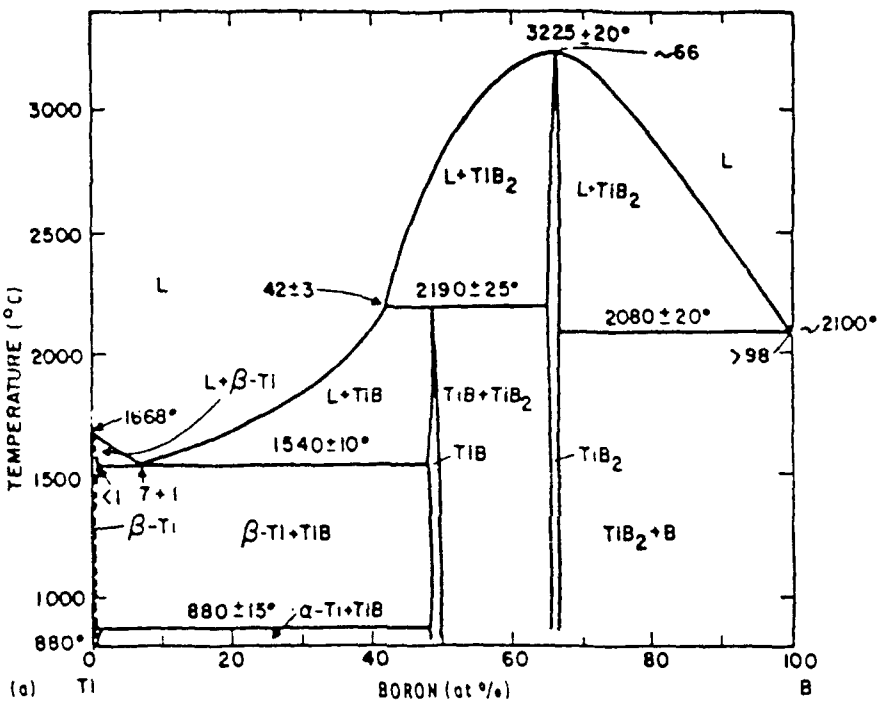

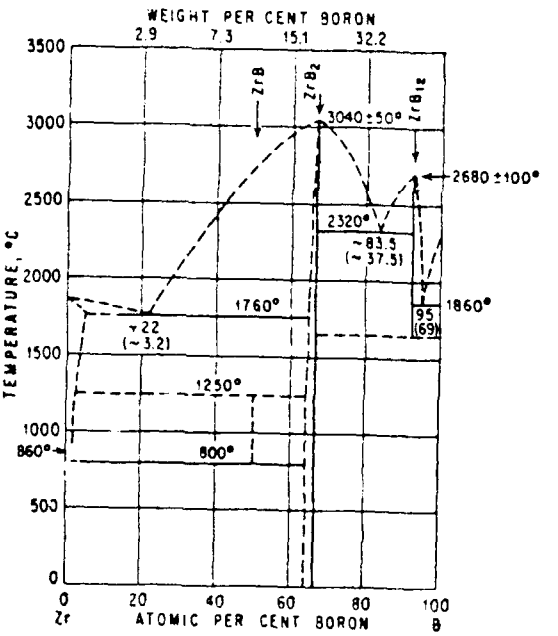

Figure 1. Phase diagrams for Ti-B and Zr-B.

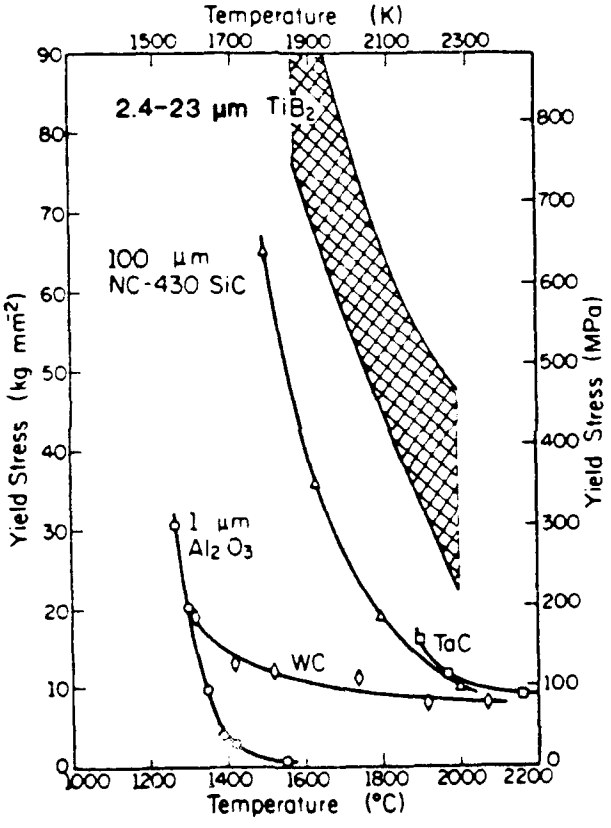

Figure 2. Yield strength of various materials as a function of temperature.

barrier layer for improving the oxidation resistance of the diborides. The oxidation of $MoSi_2$ and of composites of SiC and TiB_2 are, therefore, reviewed in sections 1.3 and 1.4

1.1 OXIDATION OF DIBORIDES

Diborides oxidize readily to form B_2O_3 which becomes a liquid at 490°C and vaporizes very rapidly above 1100°C. In addition, B_2O_3 is extremely corrosive. Several studies related to the oxidation of ZrB_2 and TiB_2 in the temperature range of 900 to 1800°C have been reported[2-7]. In the case of ZrB_2, if the oxidation occurs stoichiometrically, the reaction will be:

$$ZrB_2 + 5/2\ O_2 = ZrO_2 + B_2O_3$$

At lower temperatures (about 900 to 1100°C), the scale consists of an inner layer of ZrO_2 with an outer glassy oxide layer of B_2O_3. The reaction takes place at the oxide/diboride interface and B_2O_3 which is in liquid form diffuses through the ZrO_2 layer to the outer surface, where it volatilizes. At higher temperatures (above 1100°C), the high volatility of B_2O_3 causes disappearance of the outer glassy layer.

On the other hand, when exposed to very low pressures of oxygen, diborides are stable and do not form significant amounts of volatile species even at ultrahigh temperatures.

In order for the diborides to have any potential for applicability as reinforcement materials for composites in oxidizing envirionments, the matrix must be able to prevent penetration of oxygen to the diboride reinforcement and of B_2O_3 vapor to the surface. In addition, the matrix and the diboride must be chemically compatible at the temperatures of interest.

1.2 OXYGEN TRANSPORT THROUGH OXIDES

Although Zr_2O_3 and HfO_2 with the flourite crystal structure have high melting points, they are notorious for their high permeability to oxygen. The presence of a large void in the center of the fluorite unit cell allows

oxygen to diffuse very rapidly through these oxides. Y_2O_3 is not much better either, because of its open cubic crystal structure which is similar to the fluorite structure.

α-Al_2O_3 offers the best crystal structure for reducing oxygen transport because of its rhombohedral packing, and although it has a lower melting point (2054°C), than the other oxides, it is of particular interest in this study. However, its effectiveness as an oxygen diffusion barrier at ultrahigh temperatures is not certain. Another crystal structure which may slow oxygen transport is the perovskite structure, and hence $CaZrO_3$ is also considered for the matrix. Figure 3 shows a comparison of the diffusion of oxygen through several oxides as a function of temperaturature[8].

1.3 OXIDATION OF $MoSi_2$:

$MoSi_2$ has a melting point of 1980°C (illustrated in the phase diagram in Figure 4) and the ability to form a protective oxide coating in an oxygen environment at temperatures of interest.[9-12]

The formation of a protective SiO_2 layer above 927°C in an oxygen environment prevents the formation of the volatile SiO, MoO_2 and MoO_3 gases. This slow oxidation process is called passive oxidation. The initial reaction is:

$$MoSi_2 + 2\ O_2(g) = MoO(g) + SiO(g) + SiO_2(s)$$

until a continuous protective silica layer is formed. The oxidation of $MoSi_2$ may then follow one of these reactions:

$$5\ MoSi_2 + 7\ O_2(g) = Mo_5Si_3 + 7\ SiO_2 \text{ (non-stoichiometric)}$$

or $$2\ MoSi_2 + 7\ O_2(g) = 2\ MoO_3(g) + 4\ SiO_2 \text{ (stoichiometric)}$$

In an oxygen atmosphere, it is possible that Mo may build up at the oxid /silicide interface, oxidize and form pinholes in the viscous silica layer. Si diffuses through the matrix and reacts with oxygen at the alloy/scale interface. The SiO_2 formed above 1000°C in an oxygen environment

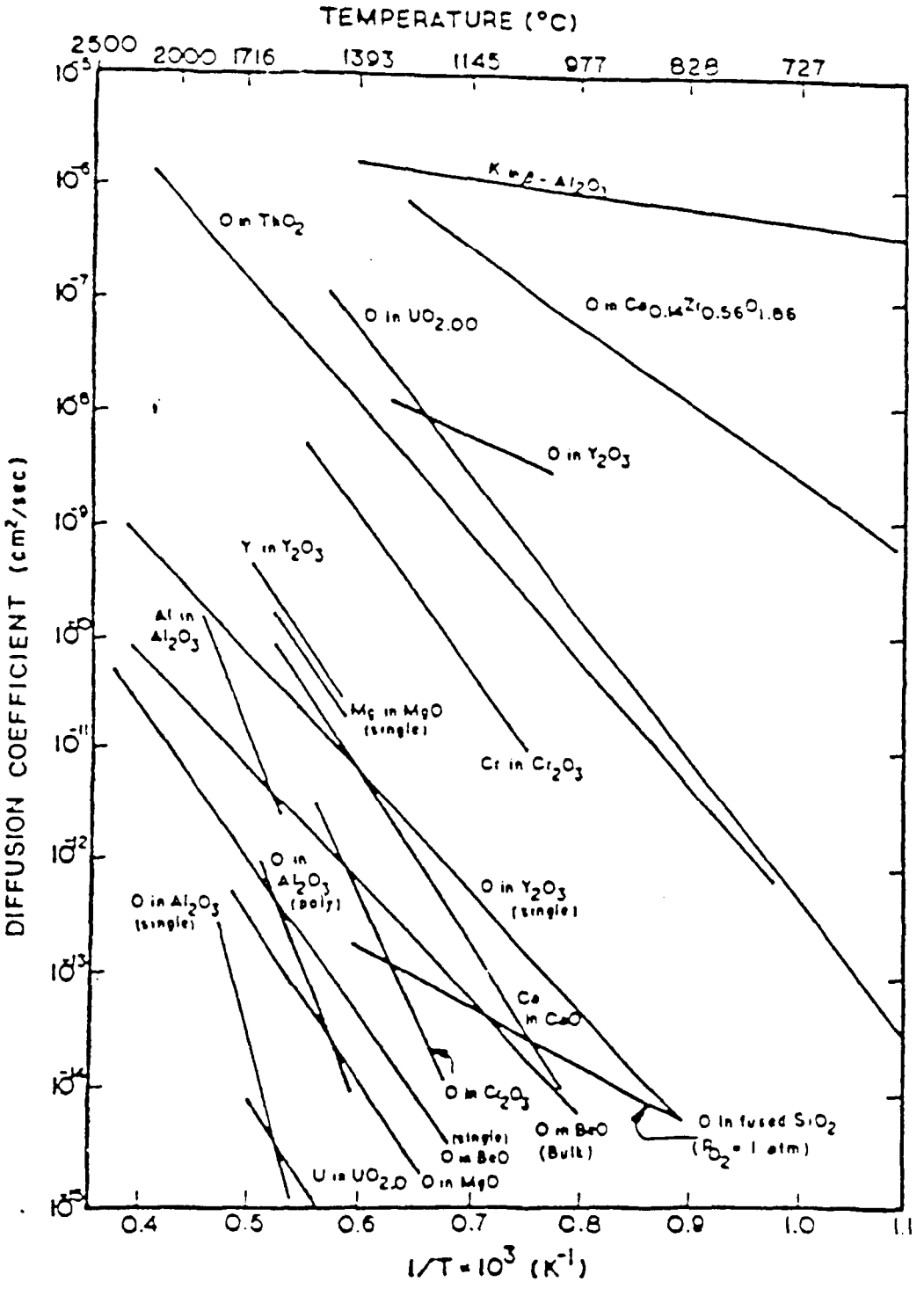

Figure 3. Diffusion data for the several oxides as a function of temperature.

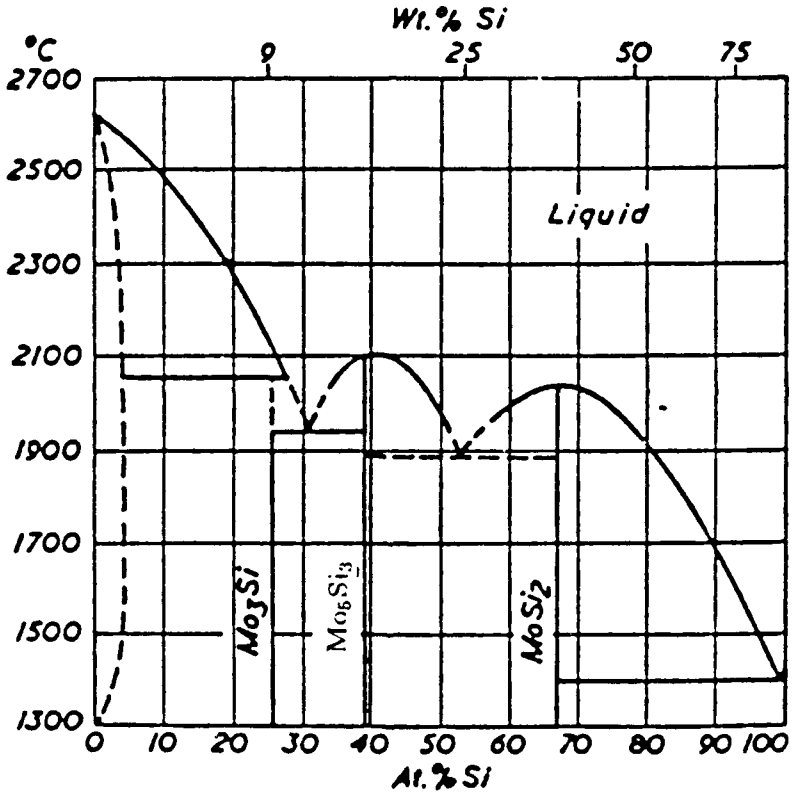

Figure 4. Phase diagram for Mo-Si.

is crystabolite up to 1500°C. The SiO_2 layer is amorphous with small regions of crystallinity at the lower end of this temperature range, and the degree of crystallinity increases with temperature. Above 1500°C, it is not clear if the silica is crystalline.

As the silica layer becomes more fluid with temperature, the diffusion of oxygen through the oxide increases, gaseous oxides accumulate at the oxide/silicide interface and leads to the failure of the silica layer.

In vacuum (i.e., at low pO_2), active oxidation occurs through rapid volatilization of SiO, leaving behind a Si depleted layer of Mo_5Si_3 on the surface, the reaction being:

$$5\ MoSi_2 + 7/2\ O_2(g) = Mo_5Si_3 + SiO(g)$$

1.4 OXIDATION OF COMPOSITES OF TiB_2/SiC:

SiC has excellent oxidation resistance up to 1650°C. It behaves very similar to $MoSi_2$ because it also forms a protective layer of silica on its surface above 1000°C. The oxidation of SiC is as follows[13,14]:

$$SiC + 3/2\ O_2(g) = SiO_2(s) + CO(g)$$

which is believed to occur by inward diffusion of oxygen to the SiC/SiO_2 interface.

The oxidation of composites of SiC reinforced with TiB_2 has been studied in the temperature range of 800 to 1400°C[15]. The initial high rate of oxidation above 1100°C is believed to be due to the oxidation of the TiB_2 particles on the surface of the composites. Although a silica layer forms on the surface, it is not very protective since the oxygen attacks the isolated TiB_2 particles on the surface of the composite and forms boria glass along with TiO_2. This fluid boria glass reacts with the viscous SiO_2 and forms fluid borosilicate glass. This fluid is able to penetrate into the matrix while the oxygen transported through the glass attack the SiC and the TiB_2 within the bulk of the composite. If less TiB_2 is encountered, the reaction would cease due to the increase in SiO_2 in the

borosilicate glass making it more viscous and reducing its ability to further penetrate the matrix.

2. OBJECTIVES

The main considerations in this program, therefore, are:

(a) The compatability between the selected diboride reinforcements and oxide matrices at ultrahigh temperatures:

(b) The ability of the selected oxides to prevent penetration of oxygen to the diboride reinforcements; and

(c) The possibility of a barrier layer of $MoSi_2$ to prevent the oxidation of the diborides at ultrahigh temperatures.

In order to accomplish this, particulate composites of selected combinations of diborides in oxide and silicide matrices were prepared and tested under a variety of conditions at ultrahigh temperatures.

3. THERMODYNAMIC CONSIDERATIONS

In order to understand the magnitude of the problems of volatilization of oxides under the conditions of interest, vapor species diagrams for B-O, Ti-O, Zr-O and Si-O have been constructed. These calculations were made using standard thermodynamic data[16]. Figure 5 illustrates the vapor pressures of the dominant vapor species as a function of pO_2 for each of these systems at 1900 K (1627°C). There is an obvious problem of very high vapor pressures of boron oxides and silicon oxides at these temperatures, even at very low partial pressures of oxygen. In the case of the oxidation of Si, in fact, the formation of volatile SiO at low pO_2 results in active oxidation whereas at higher values of pO_2 protective silica layer is able to form.

Increasing the temperature makes the situation even worse by increasing the partial pressures of the vapor species. Figure 6 illustrates the vapor pressures of the most volatile species in each of the systems B-O, Zr-O and Ti-O for 1650, 1850 and 2050°C[17]. Clearly, the amount of boria vapor formed at 2050°C is tremendous.

(a)

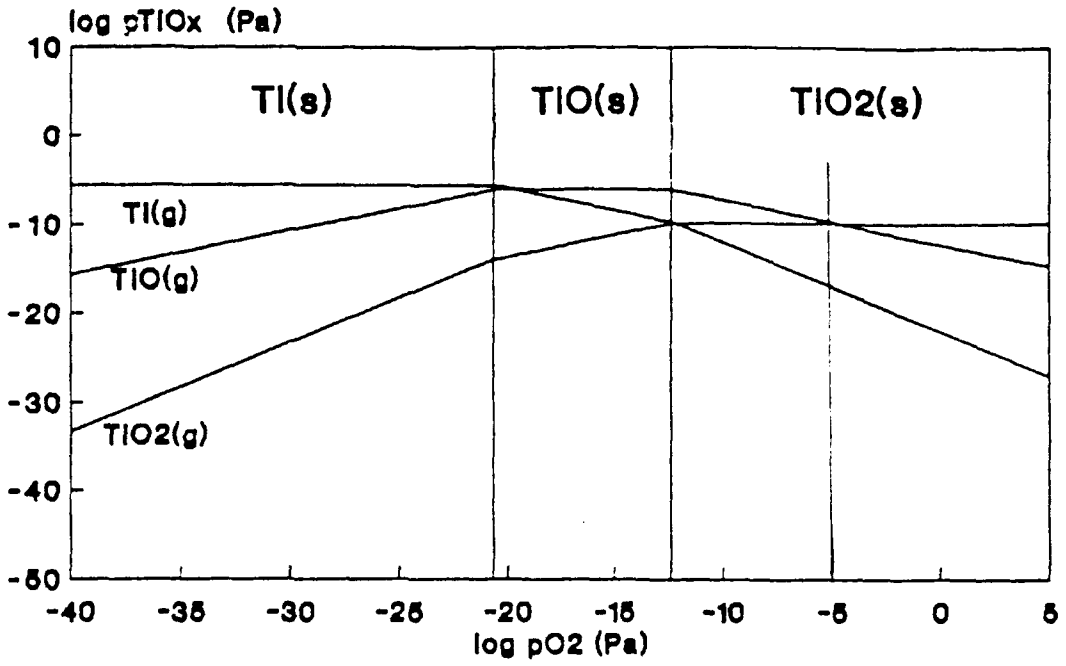

(b)

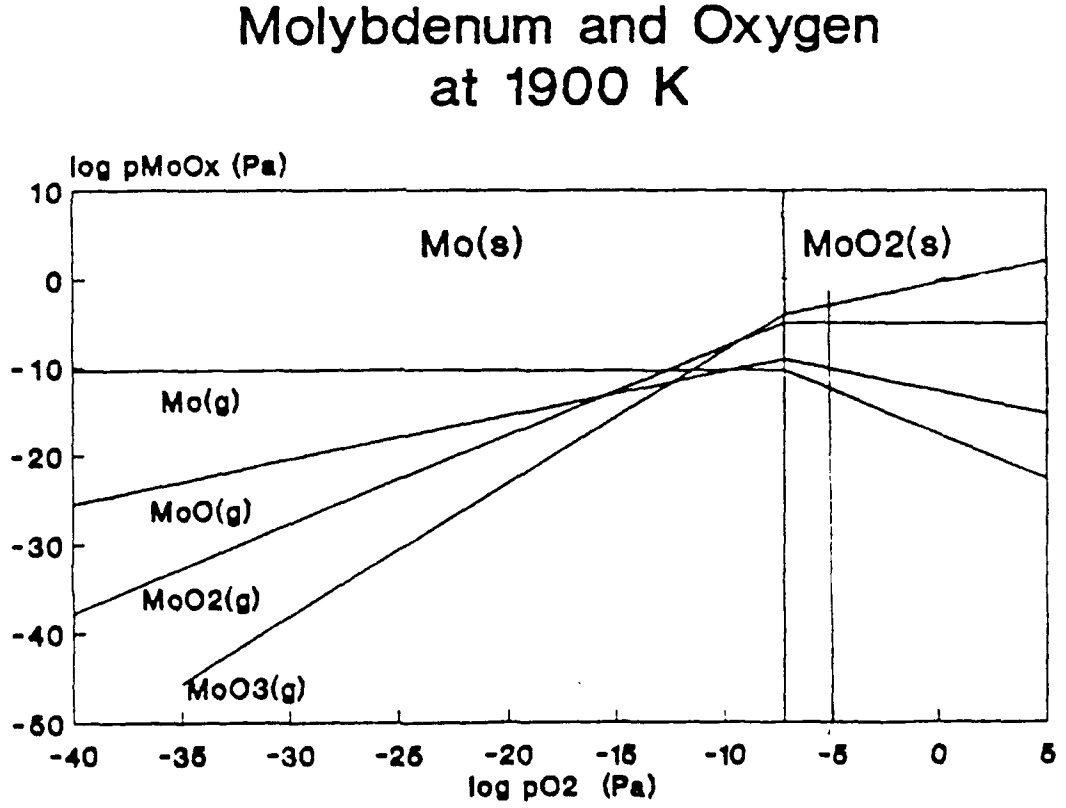

Figure 5a. Vapor species diagrams at 1900 K for (a) Ti-O, (b) Mo-O.

(c)

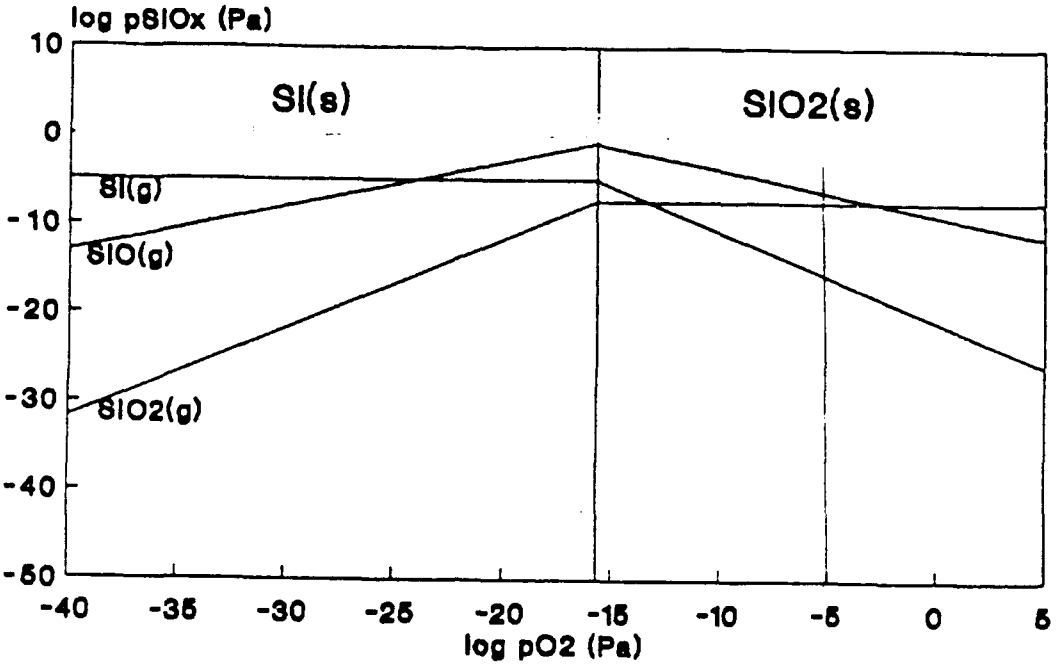

(d)

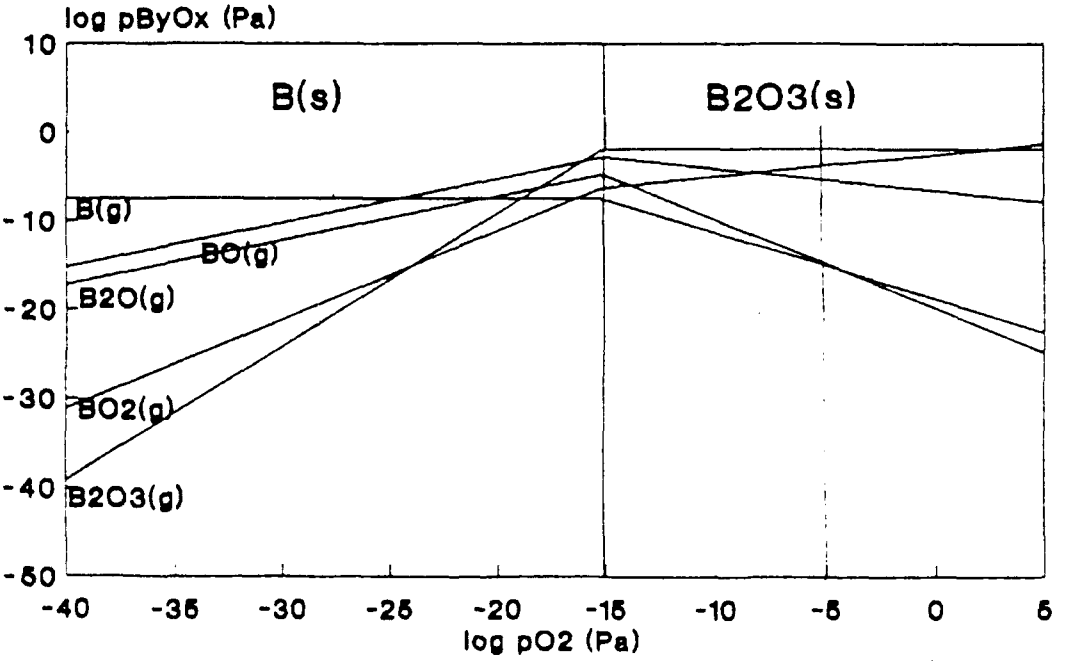

Figure 5b. Vapor species diagrams at 1900 K for (c) Si-O, (d) B-O.

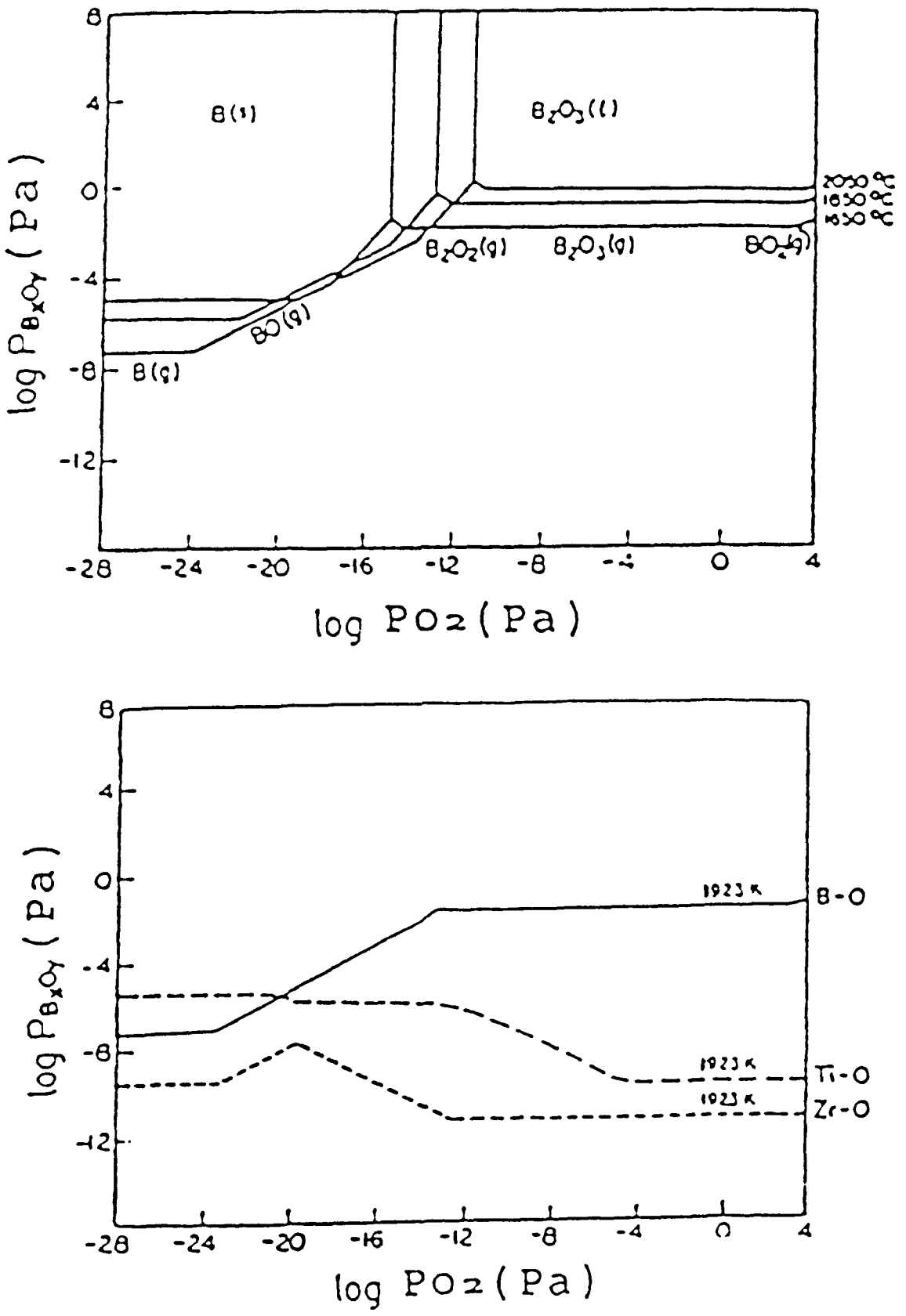

Figure 6. Diagrams for the most volatile species in B-O, Ti-O and Zr-O.

4. EXPERIMENTAL PROCEDURE

4.1 POWDER PREPARATION

TiB_2, ZrB_2, Y_2O_3 and $MoSi_2$ powders were obtained from Carboride Corporation, and fine ZrO_2 and Al_2O_3 powders were obtained from Mangesium Electron Inc. A second batch of TiB_2 powder was obtained from Union Carbide. X-ray diffraction of the powders revealed expected crystal structures except for $MoSi_2$, which contained small amounts of Mo_5Si_3, which is believed to be on the particle surfaces. Figure 7 illustrates the morphologies of some of the powders used in this study.

Suitable combinations of these powders were mechanically blended and ball milled in order to obtain the composite compacts. Seven weight percent Y_2O_3 was added to the ZrO_2 powder in order to obtain a partially stabilized structure (referred to as YS-ZrO_2 in this report). The blended mixtures were ball milled with ZrO_2 balls in an ethyl alcohol medium except in the case of the Al_2O_3 blend for which Al_2O_3 balls were used. Ball milling was carried out for 24 hours and was followed by drying in an oven. The $CaZrO_3$ was prepared by ball milling and calcining a mixture of $CaCO_3$ and ZrO_2. The calcined powder was ball milled again, along with 10% TiB_2. The $MoSi_2$ and TiB_2 powders were V-blended prior to hot pressing.

The following compacts were hot pressed:

I. Oxide Matrix Composites:

1. ZrO_2 - 7w% Y_2O_3 + 5w% TiB_2
2. Y_2O_3 + 5w% TiB_2
3. Al_2O_3 + 5w% TiB_2
4. ZrO_2 - 7w% Y_2O_3 + 5w% ZrB_2
5. Y_2O_3 + 5w% ZrB_2
6. Al_2O_3 + 5w% ZrB_2
7. $CaZrO_3$ + 10w% TiB_2

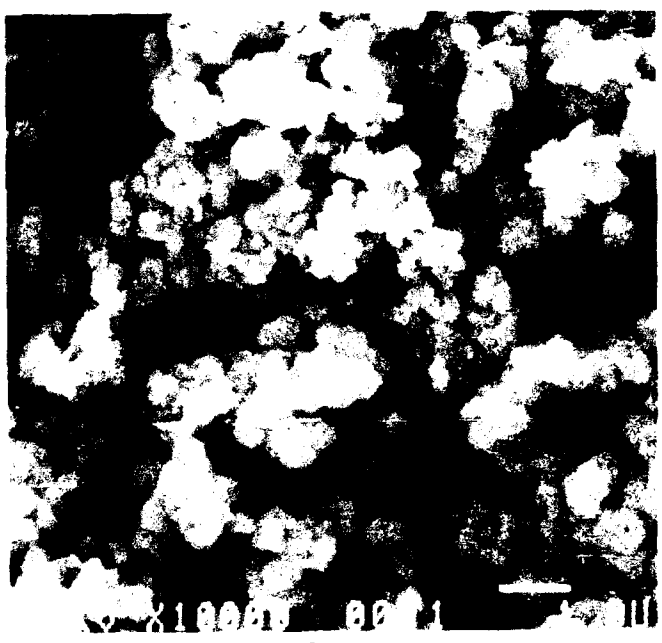

ZrO_2

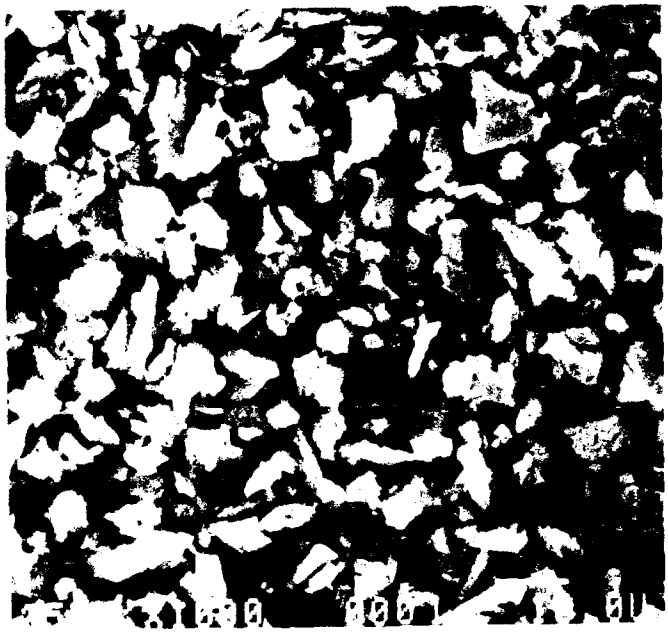

Y_2O_3

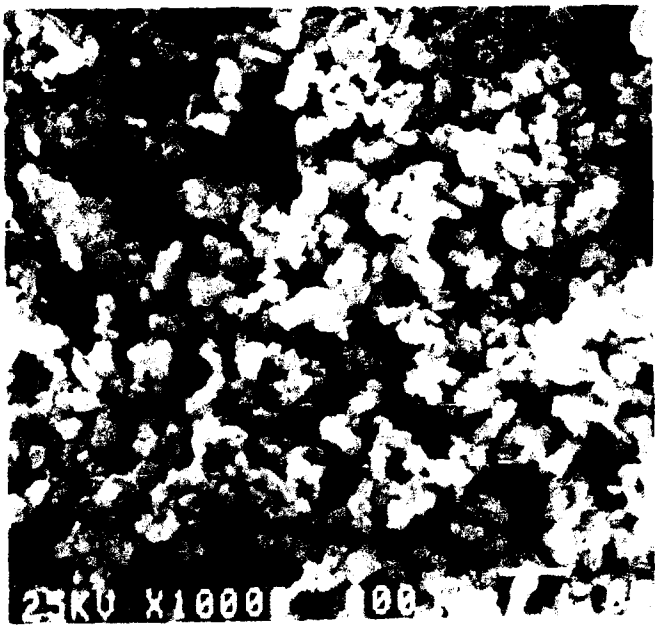

Al_2O_3

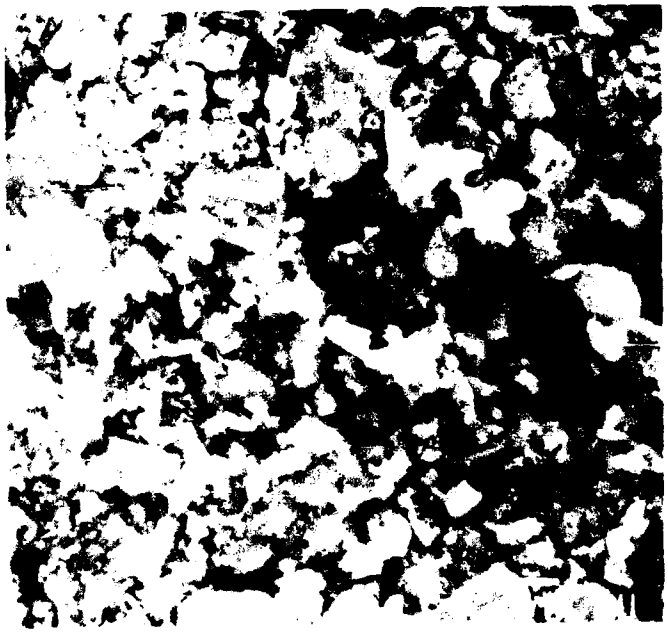

TiB_2

Figure 7a. Morphologies of the powders used in the study. ZrO_2, Y_2O_3, Al_2O_3, TiB_2.

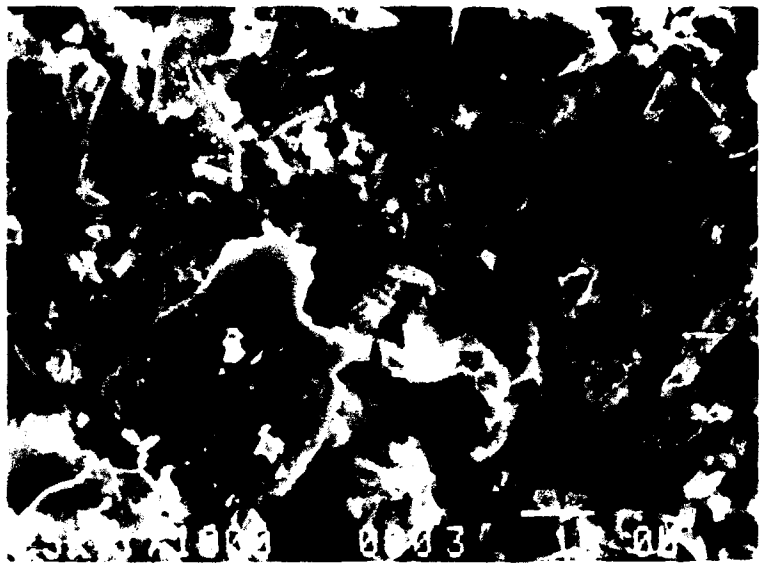

$MoSi_2$

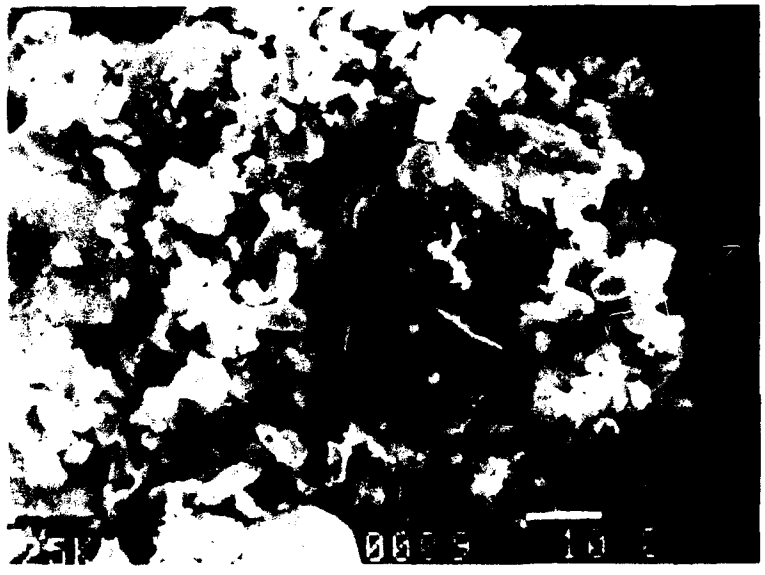

$MoSi_2$ + 20% TiB_2

Figure 7b. Morphologies of the powders used in the study. $MoSi_2$, $MoSi_2$ + 20% TiB_2.

II. Silicide and Silicide Matrix Composites:

1. $MoSi_2$
2. $MoSi_2$ + 20w% TiB_2

4.2 HOT PRESSING

The powders were vacuum hot pressed in graphite dies lined with graphfoil using graphite heating elements and the compacts were approximately 5 cm in diameter. Figure 8 illustrates a schematic of the hot pressing equipment. The assembly was first evacuated to a vacuum of about $1x10^{-5}$ torr. The temperature was increased gradually over a few hours and once the required temperature was reached, the pressure was gradually applied and maintained for the duration of the hot pressing. After the hot pressing, the pressure was released and temperature gradually decreased. Temperatures of up to 1650°C, pressures of up to 48 MPa and hot pressing times of up to 4 h were typically used. Table 1 lists details of the hot pressing conditions used for specific combinations of powders.

Some special specimens were prepared by re[illegible]sing small pieces of these composites embedded inside selected oxides. In particular, sandwich composites were made with monolithic TiB_2 embedded in $MoSi_2$ and hot pressed in an Al_2O_3 matrix in order to evaluate the potential of the $MoSi_2$ as a barrier layer.

4.3 SAMPLE PREPARATION:

The hot-pressed compacts were sectioned into samples about 5 mm x 5 mm x 5 mm using a low concentration diamond blade, in a bath containing a cutting fluid. The samples were surrounded with alumina media before polishing on a Struers Planopol, in order to prevent rounding of the edges. Grinding was performed on 200 and 600 grit diamond resin bonded wheels. The samples were then polished on pressure sensitive adhesive nylon cloths with 6, 3, 1 and 0.1 micron diamond pastes. The nylon cloth was used to prevent the pulling out of TiB_2 particles and to prevent the rounding of the edges.

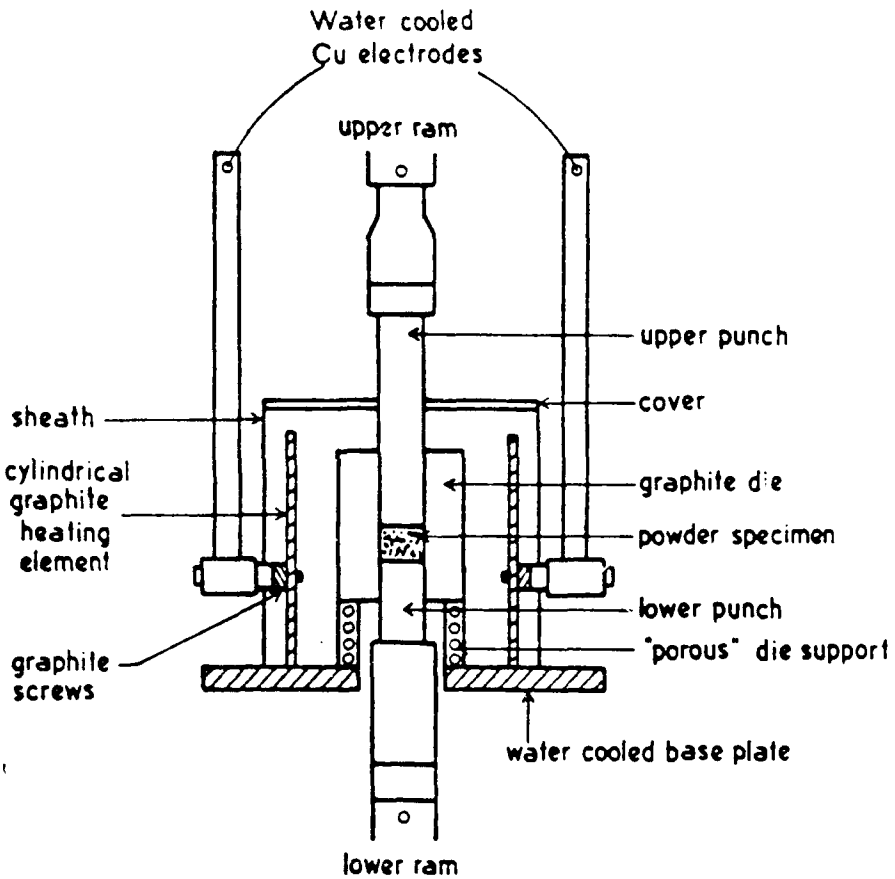

Figure 8. Schematic representation of the hot pressing equipment.

Table 1 - Hot Pressing Details

	Temperature	Pressure	Time
YS-ZrO_2+ 5w% TiB_2	1650°C	7000 psi	2 hrs
Y_2O_3 + 5w% TiB_2	1650°C	7000 psi	2 hrs
Al_2O_3 + 5w% TiB_2	1370°C	7000 psi	2 hrs
YS-ZrO_2 + 5w% ZrB_2)			
Y_2O_3 + 5w% ZrB_2)	Same as for TiB_2 composites		
Al_2O_3 + 5w% ZrB_2)			
$CaZrO_3$ + 10w% TiB_2	1650°C	7000 psi	2 hrs
$MoSi_2$	1650°C	7000 psi	1 hr
$MoSi_2$ + 20w% TiB_2	1650°C	7000 psi	1 hr

After the heat treatment, the surface layers of the samples were analyzed using microscopy and X-ray diffraction. The samples were then remounted and polished through the cross section to be examined further.

4.4 HEAT TREATMENTS:

The specific heat treatments used for the specimens are listed in Table 2.

4.4.1 In Vacuum:

Vacuum heat treatments were carried out in a Centorr furnace with Ta heating elements and Ta heat shields. The initial vacuum was about 2×10^{-7} torr which decreased to about 2×10^{-5} torr during heat up to temperature and stabilized at about 5×10^{-6} torr for most of the heat treatment time. Samples were cooled after the heat treatment at approximately 50°C per minute in vacuum. These specimens had polished surfaces which were examined by scanning electron microscopy before and after the heat treatment.

Table 2 - Heat Treatment Details

	Vacuum	Air	Oxyacetylene
YS-ZrO_2 + 5w% TiB_2	1600°C, 1 hr	1650°C, 15 min	1650, 1850, 2050°C, 1 hr
Y_2O_3 + 5w% TiB_2	"	"	
"			
Al_2O_3 + 5w% TiB_2	"	"	"
YS-ZrO_2 + 5w% ZrB_2	"	"	
Y_2O_3 + 5w% ZrB_2	"	"	
Al_2O_3 + 5w% ZrB_2	"	"	
$CaZrO_3$ + 10w% TiB_2		1475°C, 1 hr	
		1600°C, 15 mins	
		1700°C, 1 hr	
$MoSi_2$	1650°C, 2 hr	1650°C, 15 mins,	
	8 hr	1 hr, 3 hrs, 4 hrs	
$MoSi_2$ + 20w% TiB_2	1650°C, 2 hrs,	1650°C, 15 mins.	
	8 hrs	1 hr, 3 hrs, 4 hrs	

4.4.2 In Air:

Most of the air heat treatments were carried out using an induction furnace. A graphite susceptor was used around a 2.5 cm I.D. alumina tube. The susceptor was embedded in alumina powder which prevented rapid oxidation of the susceptor and provided insulation. A low density zirconia tube was used to hold the alumina powder around the graphite susceptor. Current was applied to a water-cooled copper coil which encompassed the low density zirconia tube and the temperature was raised at about 20°C per minute. Figure 9 illustrates a schematic of the induction heating assembly.

Selected specimens of the oxide-matrix composites were exposed to oxyacetylene flames in air at 1650, 1850 and 2050°C for 1 hour durations in order to evaluate their oxidation resistance.

The temperature in all experiments was measured by an optical pyrometer.

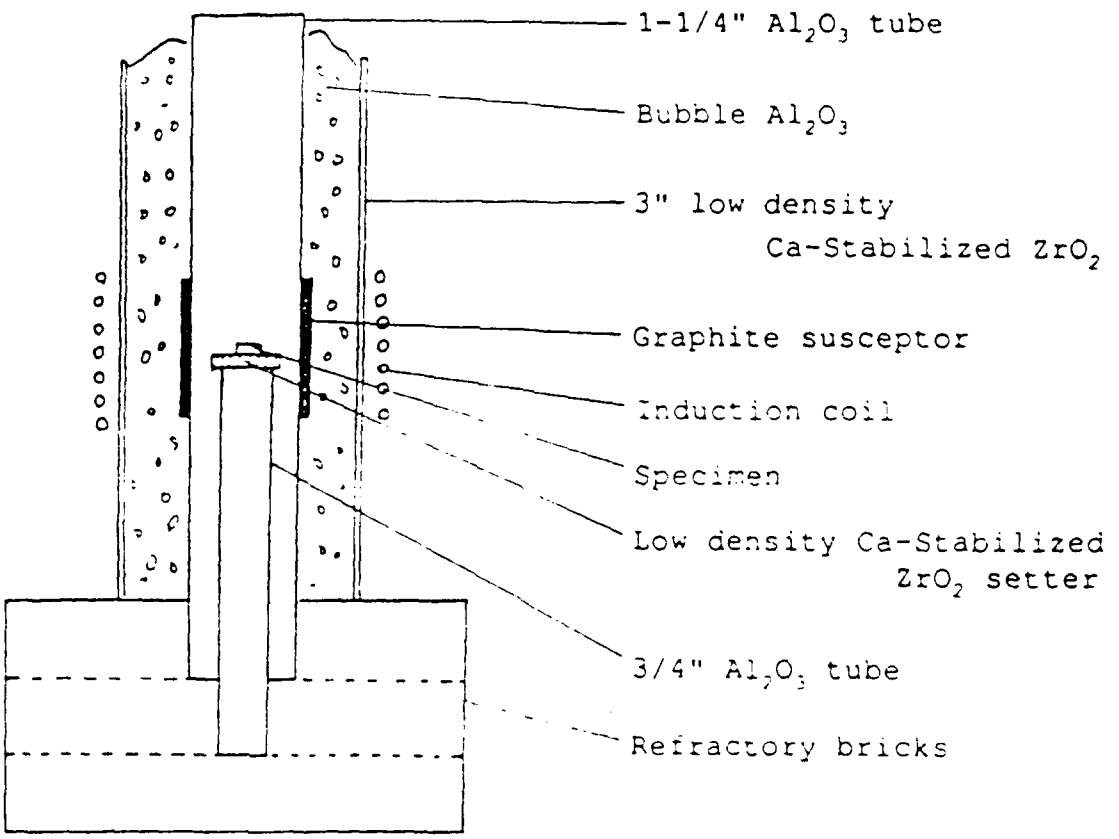

Figure 9. Schematic of the induction system used to heat treat samples in air.

4.5 EXAMINATION OF SAMPLES

The hot-pressed compacts, as well as the heat-treated compacts, were examined using a variety of techniques.

Samples were examined with a Phillips APD 3500 x-ray diffractometer using copper K radiation. Optical microscopy was carried out with a Nikon Epiphot microscope under various light conditions including reflected and polarized light. Nomarski technique was used to highlight the surface topography.

Scanning electron microscopy was carried out on a JEOL 35CF SEM and EDS on the SEM was used to obtain chemical information.

A Perkin-Elmer PHI 560 Scanning Auger Multiprobe was used to perform Auger electron spectroscopy on samples to see if reactions occurred at interfaces in the samples. However the glass phase caused charging in most of the samples and prevented significant analysis using this technique.

5. RESULTS AND DISCUSSION

5.1 OXIDE MATRIX COMPOSITES:

5.1.1 Characteristics of Hot-Pressed Composites

The composites of ZrO_2-7w% Y_2O_3 with 5w% TiB_2 and of Y_2O_3 with 5w% TiB_2, hot pressed at 1600°C and 7000 psi, had very little residual porosity. Typically within a pressing time of 2 hours a residual porosity of less than 2 percent is achieved and the diboride particles are well distributed in the matrix. The composite with Al_2O_3 as the matrix resulted in a severe reaction when hot pressed at 1600°C. However, when the hot pressing temperature was reduced to 1350°C, a satisfactory composite was obtained. The $CaZrO_3$ composites resulted in near-full density when hot pressed at 1650°C and 6000 psi for 2 hours. Typical microstructures of the as-hot-pressed YS-ZrO_2, Y_2O_3, Al_2O_3 and $CaZrO_3$ matrix composites are presented in Figure 10.

5.1.2 Chemical Compatibility in Hot Pressed Compacts

(i) YS-ZrO_2 Matrix Composites:

A close examination of the interface between the TiB_2 particles and the oxide matrix in these compacts, using scanning electron microscopy and EDAX analysis, revealed no significant reaction at the interface. The region in the matrix very close to the interface showed only Zr, suggesting negligible interdiffusion of Ti.

The expected reaction during the hot pressing would result in the formation of B_2O_3 vapor at the hot pressing temperature if adequate oxygen is available at the interface and if the products of the reaction can be transported away. The required oxygen can be obtained from ZrO_2 since this oxide exhibits large deviations from stoichiometry and is an n-type

YS-ZrO_2 + 5w% TiB_2

YS-ZrO_2 + 5w% ZrB_2

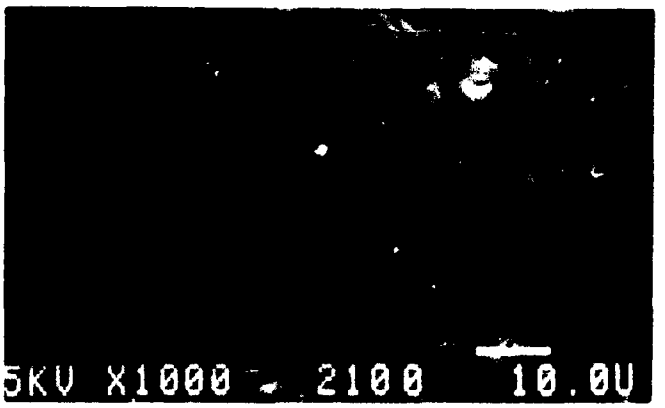

Y_2O_3 + 5w% TiB_2

Y_2O_3 + 5w% ZrB_2

Al_2O_3 + 5w% TiB_2

Al_2O_3 + 5w% $Zr\ O_2$

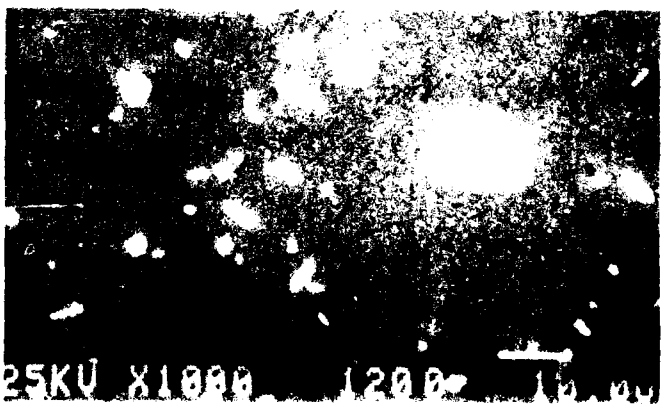

Figure 10a. Micrographs of oxide matrix composites, as-hot-pressed. YS-ZrO_2, Y_2O_3 and Al_2O_3 matrix.

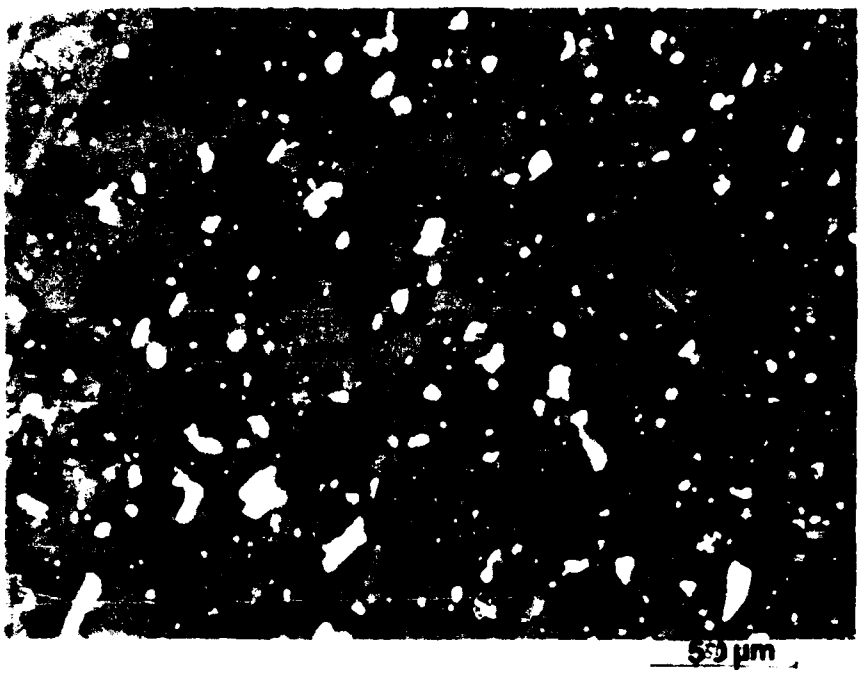

Figure 10b. Micrographs of oxide matrix composites, as-hot-pressed. $CaZrO_3$ matrix.

conductor of anions through vacancies. The reaction product, TiO_2 can dissolve in the ZrO_{2-x} on account of its high solubility as indicated in Figure 11.

B_2O_3 can, hence, form at the interface even at very low pO_2 according to the vapor species diagrams presented in Figures 5 and 6. The resulting B_2O_3 vapor can escape if proper channels or pores are available. Hence, although significant interface reactions are possible under the hot pressing conditions, the mechanical pressure applied during the processing seems to have suppressed this reaction.

A white deposit was found to have coated the inside walls of the vacuum hot press in the initial hot pressing schedules. X-ray analysis of this deposit showed it to be iron borate, suggesting that it has been formed by reaction of boric oxide vapor with the steel walls of the chamber. This reaction may have occurred during the heatup of the powder before pressure is applied since B_2O_3 vapor can escape through the pores of the loose powder. This reasoning is supported by the rapid improvement in the vacuum in the chamber as soon as the ram pressure is applied.

In most of the compacts processed for this program, the formation of the deposit was minimized by using a good vacuum system, as well as application of some pressure prior to the heatup.

(ii) Y_2O_3 Matrix Composites:

In the case of the Y_2O_3 composites as well, no obvious reaction zone was detected at the interface of the TiB_2 particles and the Y_2O_3 matrix. However, the deposit on the hot press chamber wall was present in this system as well when proper precautions were not observed, and is once again believed to be due to the reaction during the heatup.

(iii) Al_2O_3 Matrix Composites:

A severe reaction occurred during the hot pressing of this composite at 1650°C but not when pressed at 1350°C. The higher temperature is

(a)

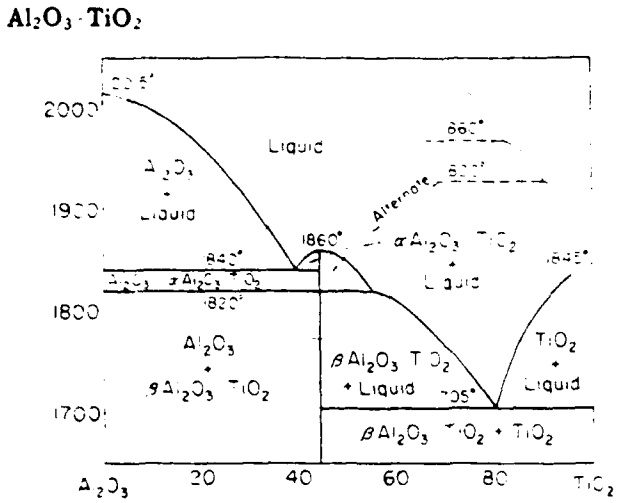

(b)

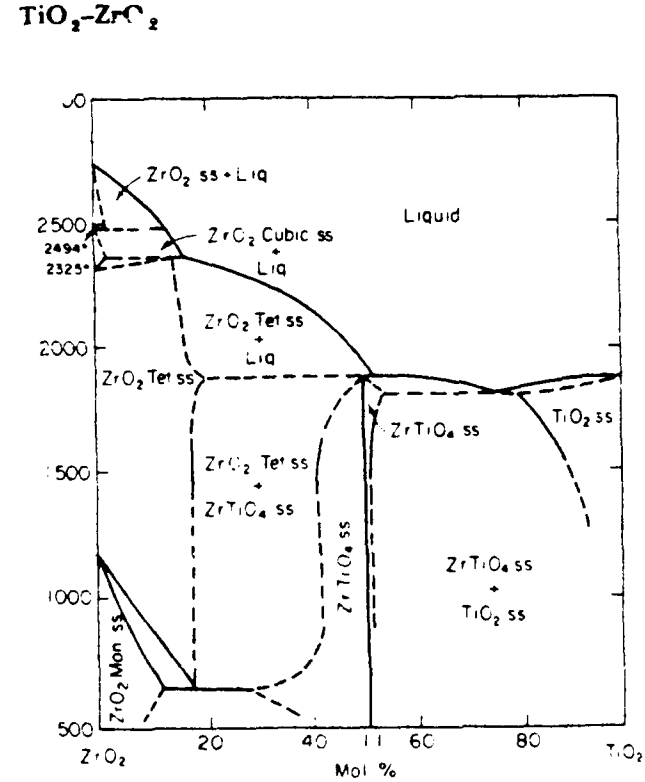

Figure 11. Phase diagrams for (a) Al_2O_3-TiO_2 and (b) ZrO_2-TiO_2.

believed to encourage the formation of aluminum carbides or aluminum oxycarbides from reaction with the graphite tooling in the hot press. In addition, a white deposit (identified as aluminum borate using X-ray analysis) was found on the chamber walls, suggesting that a reaction between Al_2O_3 and the B_2O_3 formed during the heatup.

(iv) $CaZrO_3$ Matrix Composites:

The micrographs of the $CaZrO_3$ matrix composite also show that there is no reaction between the oxide matrix and the diboride particles. This was, in fact, confirmed by very careful transmission electron microscopy. A TEM micrograph of one such TiB_2 particle in the composite is illustrated in Figure 12.

As seen from the micrographs, therefore, both the diborides are compatible with the oxide matrices, during the hot pressing. This is no evidence of significant reaction at the interface even at much higher magnifications. The problems of B_2O_3 formation in the hot pressing chamber, which were encountered in the early phases of the program, were avoided by careful control of the processing sequence.

5.1.3. Compatibility in Vacuum

The composite specimens which were exposed to vacuum, of 10^{-6} torr at 1600°C for 1 hour showed some chemical reactions at the surface. The exposed surfaces (which were polished prior to exposure) were examined on the scanning electron microscope and these surfaces are illustrated in Figure 13. Significant reaction zones are observed on the surfaces at the interfaces between oxides and diborides for the Y_2O_3 and the Al_2O_3 composites, whereas the reaction was not significant in the case of ZrO_2.

The Al_2O_3/TiB_2 interface shows evidence of grains of another phase which may be an intermediate phase between Al_2O_3 and TiO_2. No significant solubility of the two phases is expected in this system according to the phase diagram in Figure 11. The Y_2O_3/TiB_2 interface shows a definite diffusion zone which was found to contain significant amounts of

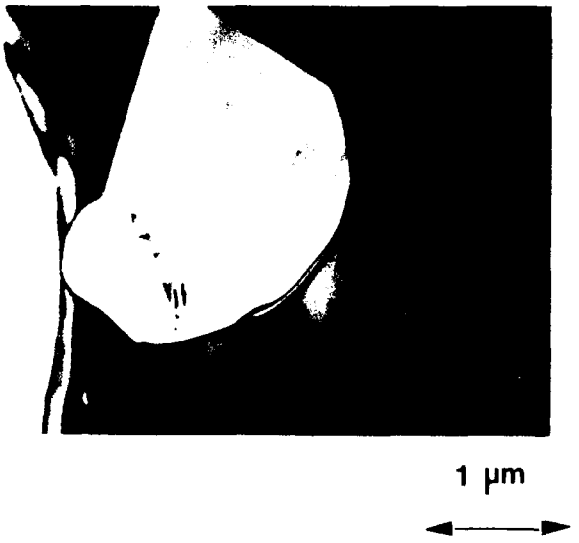

Figure 12. TEM micrograph of a TiB_2 particle in a $CaZrO_3$ matrix.

YS-ZrO_2 + 5w% TiB_2

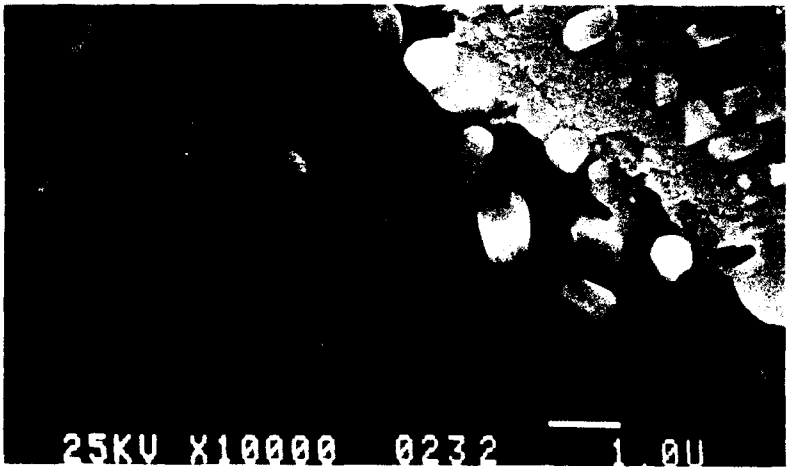

Al_2O_3 + 5w% TiB_2

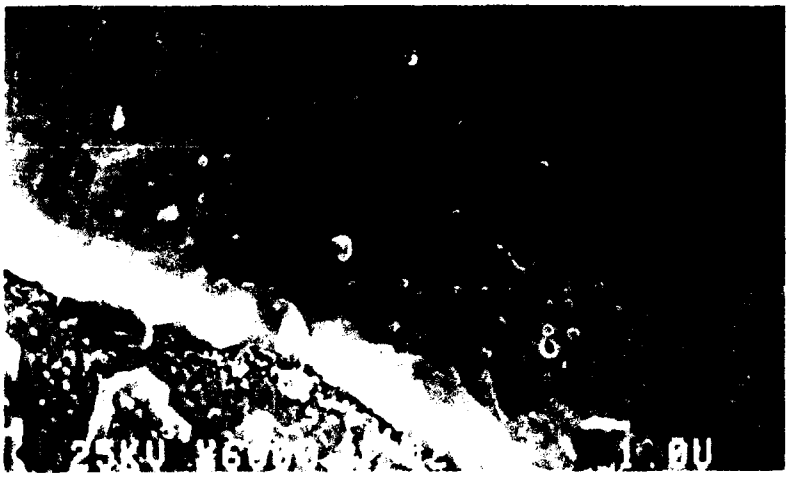

Y_2O_3 + 5w% TiB_2

Figure 13. Oxide/diboride interfaces on surface of composites vacuum treated at 1600°C, for 1 hr.

Ti. The nature of this zone is not clear. In the case of the ZrO_2 /TiB_2 interface, a solid solution of TiO_2 with ZrO_2 is expected (Figure 11) but the extent of this zone was not significant.

These results showing some reactions on the polished specimen surfaces even in vacuum are not surprising, since the thermodynamics predicts a high vapor pressure of B_2O_3 even at low pO_2 values. However, the kinetics of the reaction is dependent on the rate of arrival of oxygen to the surface and is directly proportional to the pO_2. Hence, although some surface reaction does seem to occ· · in all specimens, the rate is very slow and restricted to the surface.

Metallographic examination of cross sections of exposed specimens show no detectable reaction at the interfaces of the particles and matrices even at 1800°C. in all cases. This shows that the small amount of oxygen in the vacuum takes a long time to be transported to the interior of the compact and also confirms that the oxides and diborides, by themselves do not react to any significant extent.

5.1.4. Reactions During Induction Heating in Air

(i) YS-ZrO_2 Matrix Composites:

Specimens of YS-ZrO_2 + 5% TiB_2 and YS-ZrO_2 + 5% ZrB_2 which were induction heated in air for 15 min at 1650°C show that the composite compacts became completely porous by blistering and bloating. Micrographs in Figure 14 illustrate these porous compacts. Evidently the formation of B_2O_3 was very rapid and the vapor forced its way out. The pores in the compact with TiB_2 are smaller than those with ZrB_2 and this may be due to the formation of TiO_2 which can dissolve up to 20% in the ZrO_2 matrix and lower its melting point and presumably its strength. X-ray analysis of the compact revealed some $ZrTiO_4$ but no Zr or Ti borates. The ZrB_2, on the other hand, is changed to the matrix phase ZrO_2. Another factor contributing to the difference in the behavior of ZrB_2 and $Ti3_2$ may be the volatility of TiO.

YS-ZrO_2 + 5w% TiB_2

YS-ZrO_2 + 5w% ZrB_2

Y_2O_3 + 5w% TiB_2

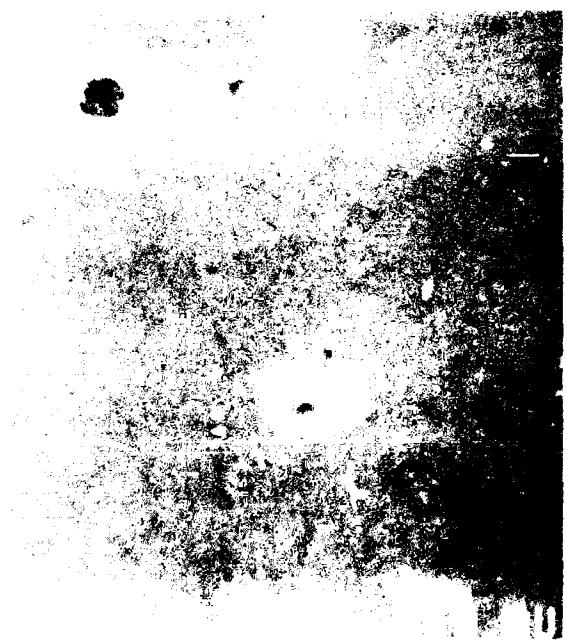

Y_2O_3 + 5w% ZrB_2

Figure 14. Micrographs of sections of YS-ZrO_2 and Y_2O_3 matrix composite specimens heat treated in air at 1650°C for 15 min.

(ii) Y_2O_3 Matrix Composites:

The Y_2O_3 + 5% TiB_2 and Y_2O_3 + 5% ZrB_2 composites also became very porous when induction heated in air for 15 min at 1650°C. However, in these specimens the porosity was less severe, although larger and more isolated (as illustrated in Figure 14). At the same time, a large amount of liquid phase is evident in the microstructure and this liquid phase caused the sample to lose its shape during the heat treatment. The isolated and rounded pores left behind in the Y_2O_3 matrix suggest that the B_2O_3 cannot force its way out of the Y_2O_3 as readily as in the ZrO_2 matrix. Observation of the sample during the heat treatment showed that it loses shape suddenly at just below 1650°C, and this must be the onset of the formation of the liquid phase. X-ray analysis revealed significant amounts of low melting Y_3BO_6 and Y_2TiO_5 in the sample, which may be the liquid phase observed in the microstructure. Figure 15 illustrates part of the phase diagram for Y_2O_3-B_2O_3.

(iii) Al_2O_3 Matrix Composites:

The Al_2O_3 + 5% ZrB_2 composites are the most promising since when induction heated for 15 min at 1650°C, the specimens did not blister or bloat. The specimens only changed color from the grey of the hot-pressed samples to the white expected for Al_2O_3. This was due to oxygen pickup and the extent of the transport of oxygen could be traced by a transition in the color across the cross section. Figure 16 illustrates micrographs of the inner and outer zones for the two composites.

Although macroscopically the compact looks intact, microscopic examination revealed that the outer zone was very porous in the TiB_2 sample and contained evidence of interconnected liquid phase in the ZrB_2 sample. The inner region for the TiB_2 composite contained evidence of reactions and the formation of a liquid phase even though the matrix Al_2O_3 did not pick up oxygen (as indicated by absence of change in color). This suggests short circuit transport of oxygen through the interconnected liquid phase. The inner region of the ZrB_2 sample, nevertheless, remained intact.

(a)

(b)

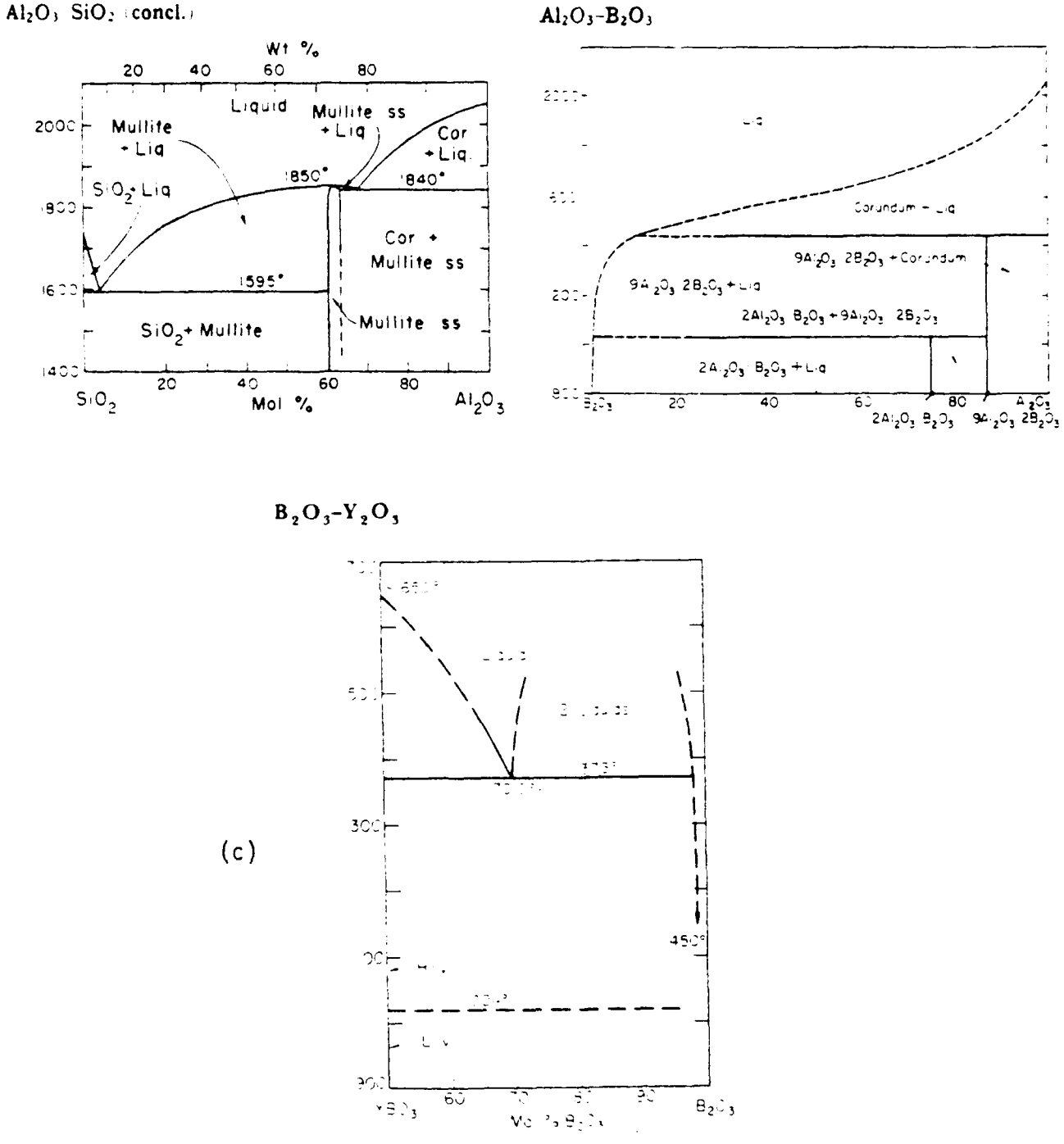

B_2O_3-Y_2O_3

(c)

Figure 15. Phase diagrams for (a) Al_2O_3-SiO_2, (b) Al_2O_3-B_2O_3 and (c) Y_2O_3-B_2O_3.

Al_2O_3 + 5w% TiB_2

Outer Zone

Inner Zone

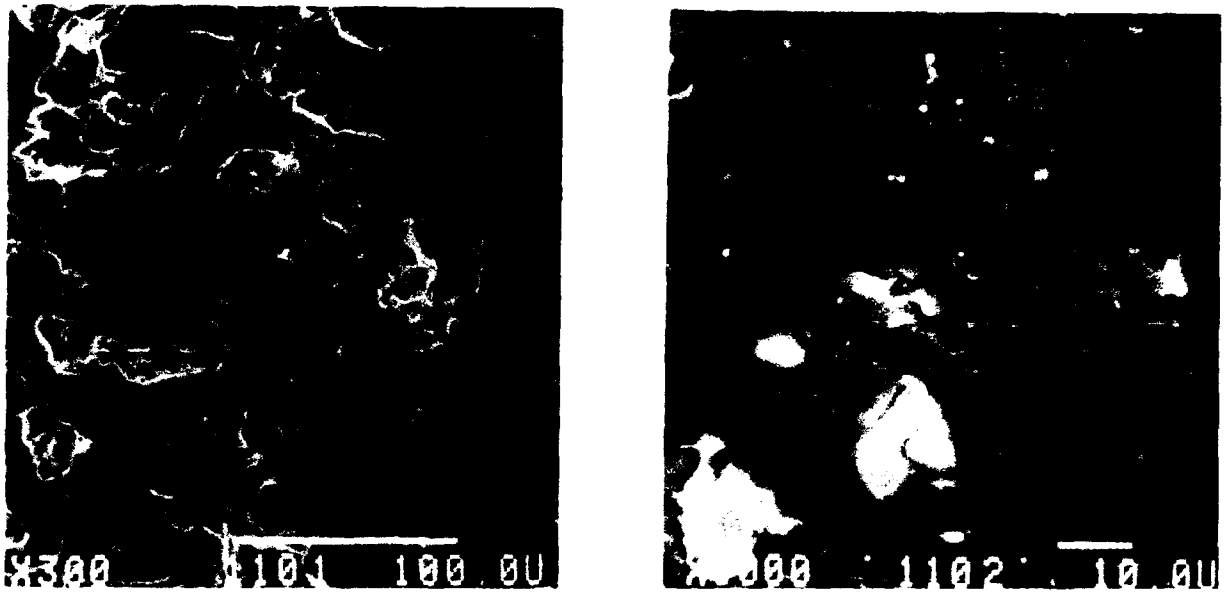

Al_2O_3 + 5w% ZrB_2

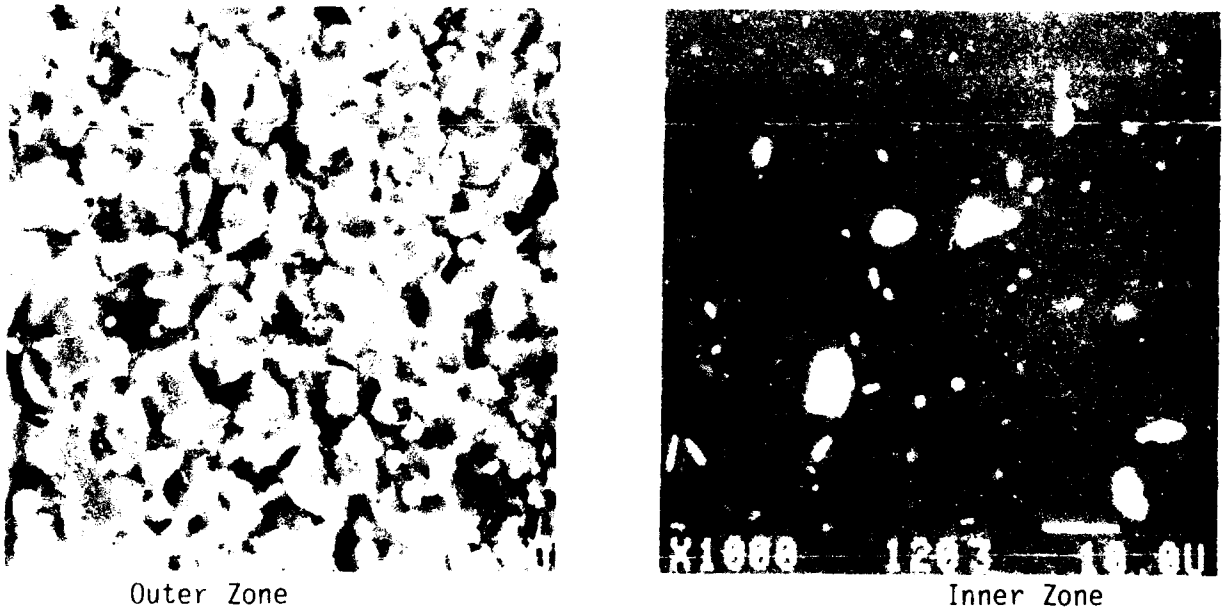

Outer Zone

Inner Zone

Figure 16. Micrographs of sections of Al_2O_3 matrix composite specimens heat treated in air at 1650°C for 15 min.

The severity of the reaction during induction heating in air at 1650°C is, hence, less in the case of the ZrB_2 composite than in the case of the TiB_2 composite.

(iv) $CaZrO_3$ Matrix Composites:

Specimens of $CaZrO_3$ matrix composites when heat treated by induction in air at 1475°C for 1 h, at 1600°C for 15 min and at 1700°C for 1 h, showed significant reactions as illustrated in Figure 17.

The specimen which was heat treated at 1475°C (Figure 17a) shows the transition between the reacted zone and the unreacted zone. In the reacted zone a significant amount of liquid phase has formed and consumed most of the diboride particles. In the unreacted zone the diboride particles are essentially intact. With more time, this part of the compact will also be expected to react.

The specimen which was exposed at 1600°C (Figure 17b) showed a similar reacted zone as in the specimen exposed at 1475°C. The depth and severity of the zone was, however, more significant. SEM/EDS analysis of the regions of the matrix around the diboride particles in the transition zone shows that regions surrounding TiB_2 particles are depleted in Ca, suggesting that CaO may have been lost. It is not clear, however, where this CaO has gone.

The specimen exposed at 1700°C has none of the diboride particles left in their original form. A liquid phase network surrounding the $CaZrO_3$ particles is observed (Figure 17c) and is believed to be a combination of B_2O_3 as well as $Ca(Zr,Ti)O_3$, which melts at about 1700°C.

It, therefore, appears that $CaZrO_3$ is superior as a matrix compared with either ZrO_2 or Y_2O_3, since it does not allow the B_2O_3 to bubble away leaving behind a porous network. This must be due to its perovskite crystal structure. However the diborides do react with the matrix in the presence of oxygen, resulting in a reaction zone with a large amount of liquid phase, particularly at higher temperature.

(a) 1475°C, 1 h

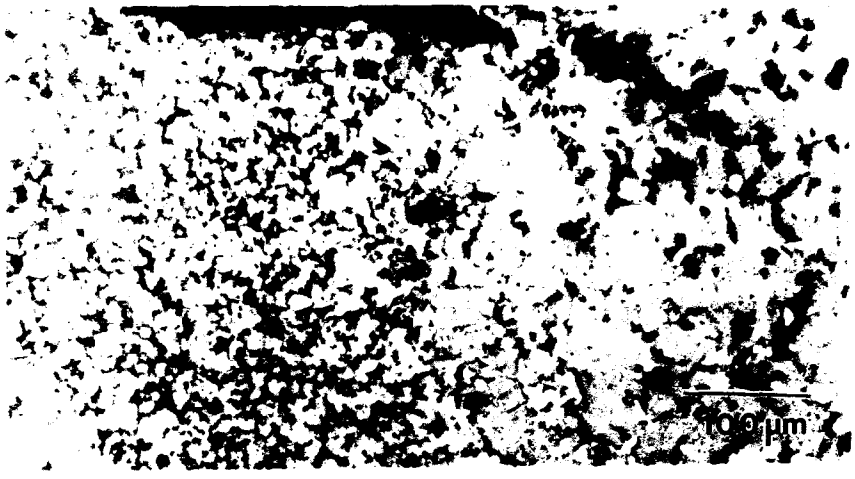

(b) 1600°C, 15 min

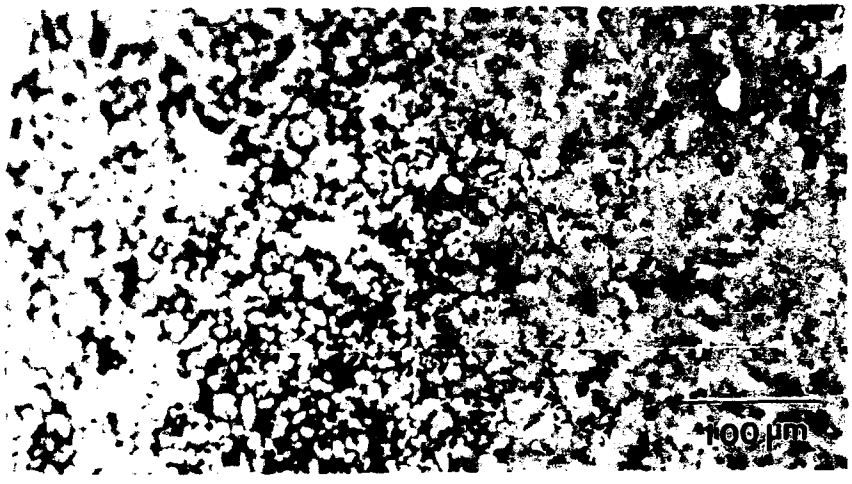

(c) 1700°C, 1 h

Figure 17. Sections of $CaZrO_3$ matrix composite specimens heat treated in air (a) 1475°C for 1 h, (b) 1600°C for 15 min and (c) 1700°C for 1 h.

5.1.5. Oxidation Reactions in Oxyacetylene Flames

When the specimens of ZrO_2-7w%Y_2O_3 + 5w%TiB_2 were exposed to oxy-acetylene flames at 1650, 1850 and 2050°C for 1 h, all specimens developed large blisters on the surfaces. The extent of the area covered by blisters, as well as the size of the individual blisters, increased with increasing oxidation temperature. In addition to the blisters, the exposed surfaces were characterized by a glassy appearance.

The oxidized specimens revealed a large amount of porosity, the size and severity of the porosity increasing with increasing temperature of treatment. A cross section of the specimen exposed at 1650°C is shown in Figure 18a and schematically represented in Figure 18b. Figure 19 illustrates the cross section of specimens exposed at 1850 and 2050°C. A gradient in the pore sizes is observed, with the pores being larger and more severe near the top surface directly exposed to the flame. The size and distribution of the pores at the bottom of the specimens correspond well with the size and distribution of the original TiB_2 particles in the unoxidized composite samples.

The Ti diboride particles have completely reacted with the oxygen from the atmosphere. The titanium oxide forms a solid solution with the zirconia matrix and the B_2O_3 vapor is lost to the atmosphere. Wavelength dispersive analysis of the matrix for boron confirms that the level of boron in the matrix and in the pores is not significant. The dissolution of significant amounts of titanium in the zirconia is confirmed by the EDX analysis. Furthermore, the concentration of Ti increases in the matrix towards the surface exposed to the flames and makes the zirconia near the top of the specimen translucent. The exposed surface layer is also characterized by the presence of glassy beads, which are suspected to be titanium rich zirconia which has a lower melting point than that of pure zirconia.

The removal of B_2O_3 in the form of vapor results in the formation of pores at the sites of the diboride particles. Due to the pressure buildup in the pores, the pore size increases and pore coalescence takes place

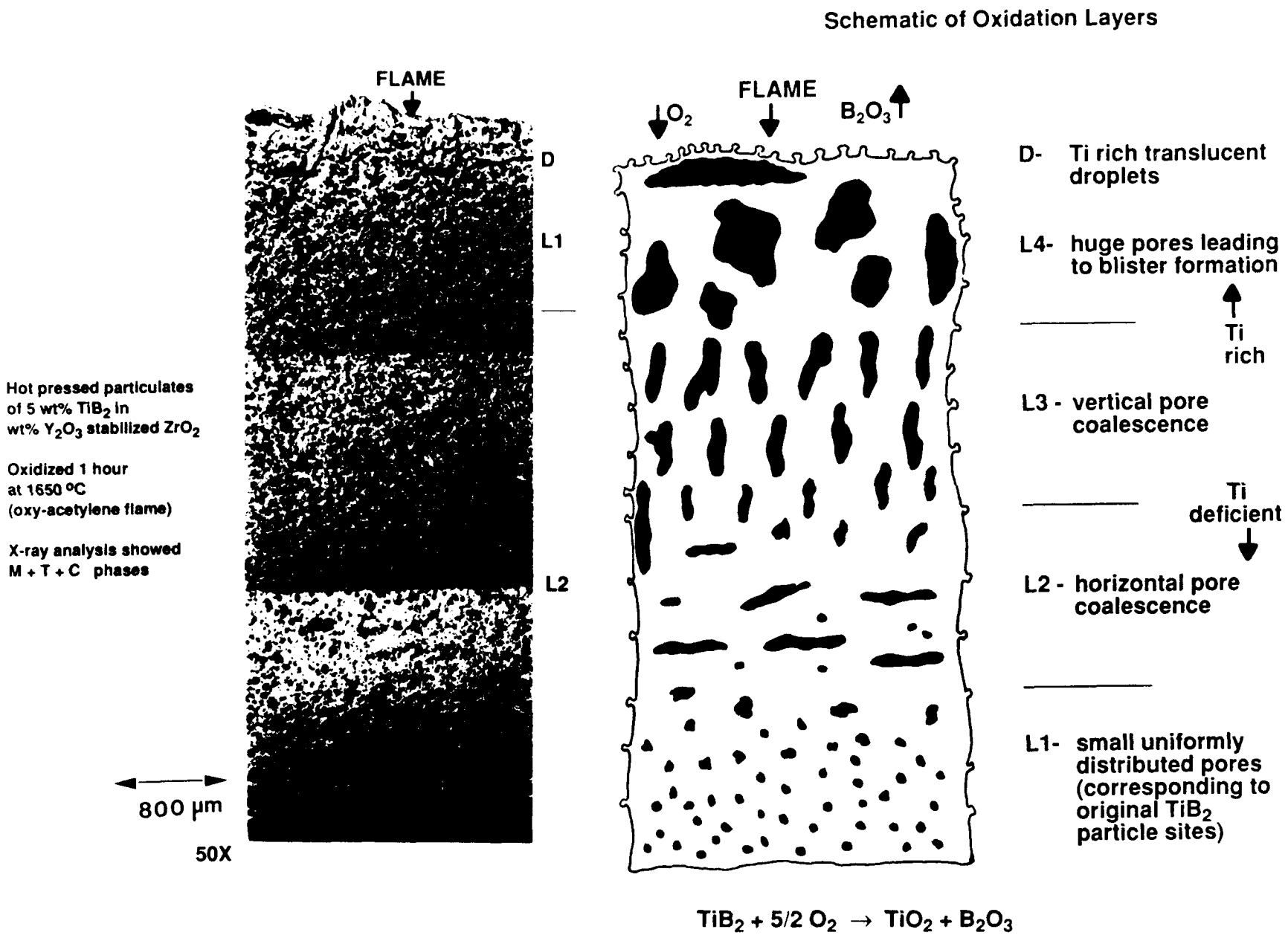

Figure 18. YS-ZrO_2 matrix composite specimen heat treated in oxyacetylene flames at 1650°C for 1 h: (a) micrograph and (b) schematic.

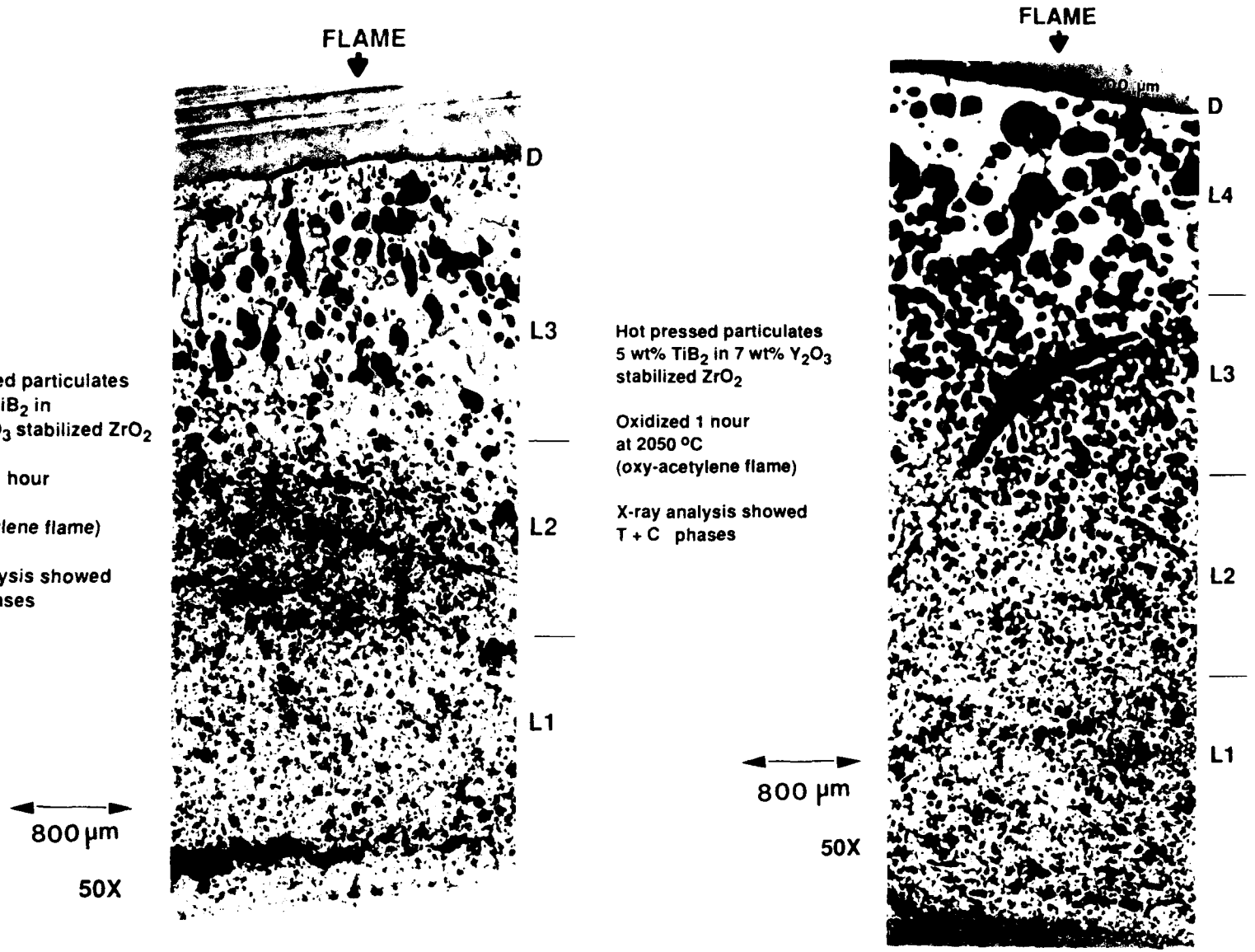

Figure 19. Sections of YS-ZrO_2-matrix composite specimens heat treated in oxyacetylene flames at (a) 1850°C and (b) 2050°C for 1 h.

at higher temperatures and nearer the exposed surface. The transport of B_2O_3 is through an interconnected network of pores created by the pressure of buildup. In addition, the poor thermal shock resistance of ZrO_2 will increase the likelihood of developing cracks and channels during the exposure, through which not only can the B_2O_3 escape, but more catastrophic ingress of oxygen can occur.

5.2. SILICIDE MATRIX COMPOSITES

5.2.1. Chemical Compatibility in Hot-Pressed Compacts:

Typical microstructures of the $MoSi_2$ compact and the $MoSi_2$ + 20% TiB_2 composite compacts using polarized light and Nomarski technique are illustrated in Figure 20. X-ray diffraction has shown small amounts of Mo_5Si_3 in both the compacts, and traces of MoB in the composite compact, indicating some reaction of the $MoSi_2$ with the TiB_2 during the hot pressing. However, the higher magnification microstructure (illustrated in Figure 21) does not reveal any obvious reaction zone. Upon closer examination using EDS mapping of elements, some of the darker regions of this microstructure have been identified as Si rich, suggesting the presence of a silica phase at the interface between the TiB_2 and the $MoSi_2$. Table 3 lists the details of the X-ray analysis of the specimens.

5.2.2. Compatibility in Vacuum

(i) $MoSi_2$:

The $MoSi_2$ specimen heat treated in vacuum showed an increased amount of Mo_5Si_3 and some Mo on the surface along with porosity, indicating active oxidation of Si in the form of SiO vapor which is removed by the vacuum. Thermodynamically, SiO vapor can exert a significant vapor pressure under these conditions. This is similar to the case of oxidation silicon. Figure 22 illustrates the cross sections of samples of $MoSi_2$ heat treated in vacuum at 1650°C, for 2 hours and 8 hours respectively. EDS

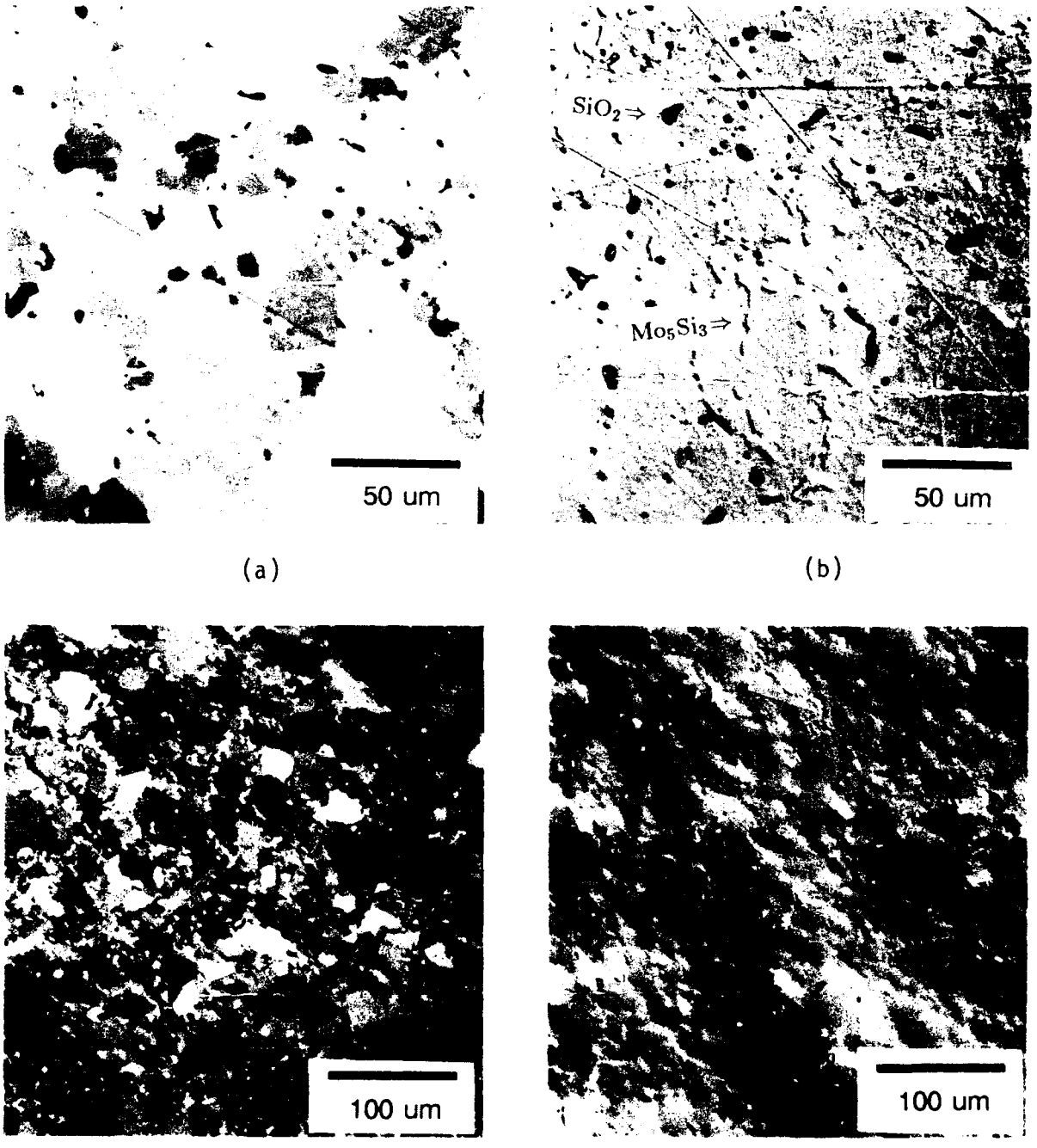

Figure 20. Micrographs of hot-pressed $MoSi_2$: (a) Polarized, (b) Nomarski and $MoSi_2$ + 20% TiB_2, (c) Polarized, and (d) Nomarski.

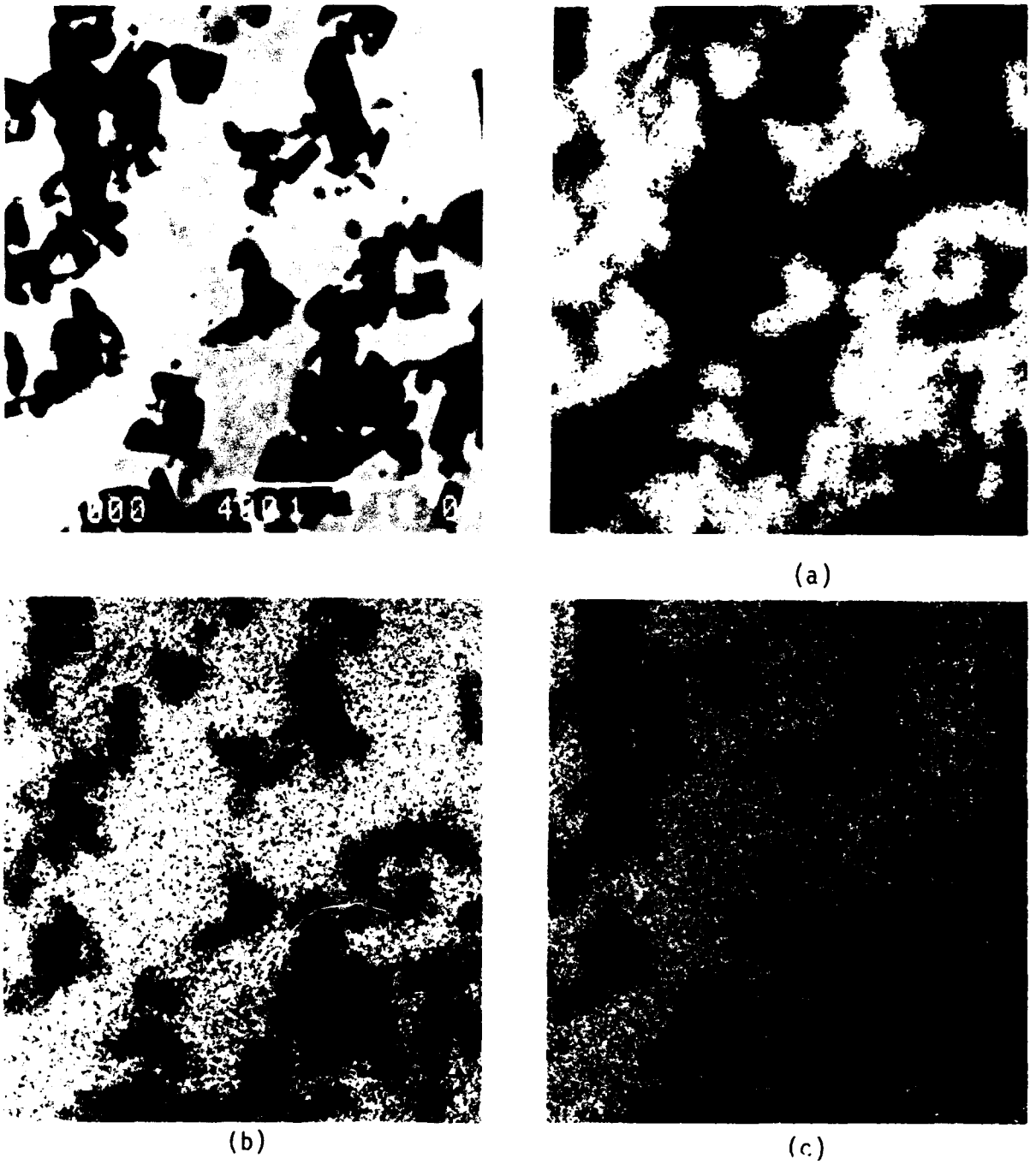

Figure 21. Micrographs and EDS maps of hot-pressed $MoSi_2$+20% TiB_2 composite. (a) Ti map, (b) Si map and (c) Mo map.

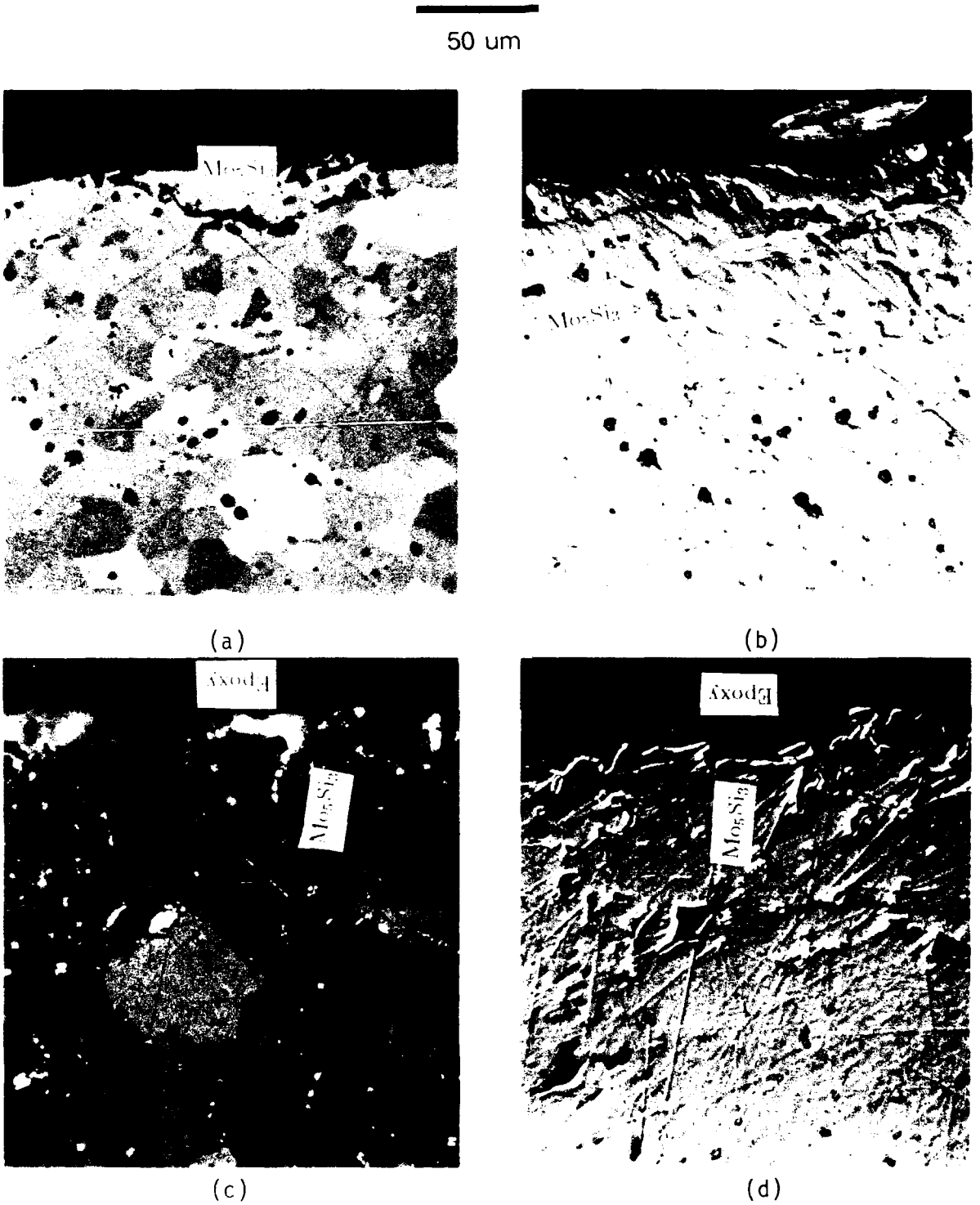

Figure 22. Micrographs of specimens of $MoSi_2$, heat treated in vacuum at 1650°C for (a) 2 h (Polarized), (b) 2 h (Nomarski), (c) 8 h (Polarized), and (d) 8 h (Nomarski).

Table 3 - Results of X-ray Diffraction Analysis of $MoSi_2$ and $MoSi_2$ + 20% TiB_2 Specimens.

Condition	Area	Composite	$MoSi_2$
Powder		S-$MoSi_2$ m-TiB_2 w-Mo_5Si_3	S-$MoSi_2$ w-Mo_5Si_3
As-Hot Pressed		S-$MoSi_2$,m-TiB_2, vw-Mo_5Si_3	S-$MoSi_2$, vw-Mo_5Si_3
Air 15 min at 1650°C	Surface	S-TiO_2, w-$MoSi_2$	S-$MoSi_2$, w-SiO_2, w-Mo_5Si_3
	Cross Section	As-HP	As-HP
Air 1 hour at 1650°C	Surface	S-TiO_2 w-$MoSi_2$	S-$MoSi_2$, w-SiO_2, w-Mo_5Si_3
	Cross Section	As-HP	As-HP
Air 4 hours at 1650°C	Surface	VS-TiO_2 vw-$MoSi_2$	S-$MoSi_2$, w-Mo_5Si_3
	Cross Section	As-HP	As-HP
Vacuum 2 hours at 1650°C	Surface	S-MoB, S-Mo_5Si_3, w-TiB_2	S-Mo_5Si_3, m -$MoSi_{0.65}$
	Cross Section	As-HP, vw-MoB	S-$MoSi_2$, w-Mo_5Si_3
Vacuum 8 hours at 1650°C	Surface	S-MoB vw-TiB_2, vw-Mo_5Si_3	S-Mo_5Si_3
	Cross Section	As-HP, vw-MoB	S-$MoSi_2$, m-Mo_5Si_3

definitions: As-HP : the x-ray pattern was similar to the as-hot pressed
VS- : the x-ray peaks of this material were very strong
S- : the x-ray peaks of this material were strong
m- : the x-ray peaks of this material were medium
w- : the x-ray peaks of this material were weak
vw- : the x-ray peaks of this material were very weak

mapping of an area (illustrated in Figure 23) clearly reveals the Si-depleted layer of Mo_5Si_3 beneath the surface formed as a result of the active oxidation of Si.

(ii) $MoSi_2$ + 20% TiB_2:

When the composite containing TiB_2 is exposed to vacuum, active oxidation is again observed just as in the case of the $MoSi_2$. A reaction zone near the surface shows porosity where not only has the Si oxidized, but the TiB_2 particle near the surface have oxidized and vaporized. Figures 24a and b illustrate cross sections of the composite compact specimens exposed for 2 h and 8 h to vacuum at 1650°C. The presence of the TiB_2 particles in the $MoSi_2$ has increased the reaction zone to some extent although not dramatically. Table 4 compares the depths of the reaction zones for the monolithic and composite compacts, and shows that the active oxidation of the Si is not modified significantly by the presence of the diboride. An interesting observation based on EDS mapping of the cross section of the sample exposed for 8 h (Figure 25), is the presence of a thin layer of MoB (confirmed by X-ray diffraction) under the surface, but above the Mo_5Si_3 layer.

5.2.3. Reactions During Induction Heating in Air:

(i) $MoSi_2$:

When the $MoSi_2$ is exposed to air instead of vacuum, a glassy layer forms on the surface and this layer appears to slow further reaction with the air. Some crystalline SiO_2 is found within this glassy layer and the microstructure indicates passive oxidation by formation of a protective silica glass on the surface. Figure 26 illustrates the formation of a glassy layer on the surface of $MoSi_2$ heat treated in air for 15 m, 1 h and 4 hours. When these samples are polished at a slight angle to partly remove the glassy layer, the grain structure of the underlying $MoSi_2$ is clearly evident as illustrated in Figure 27. This suggests that an

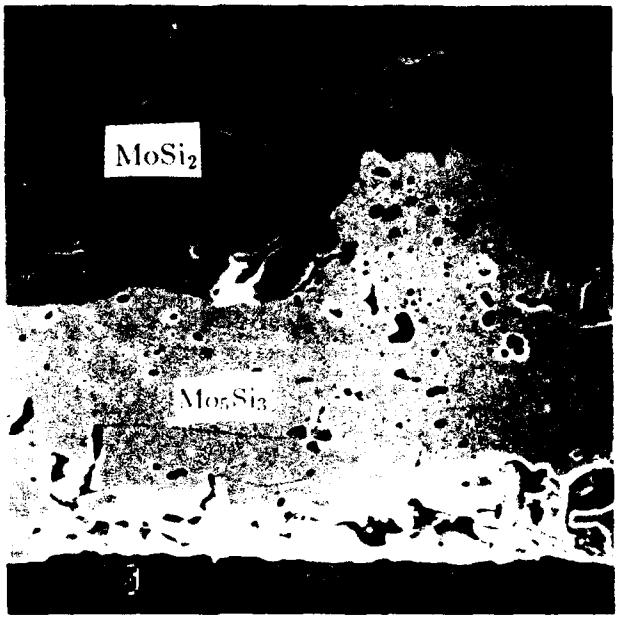

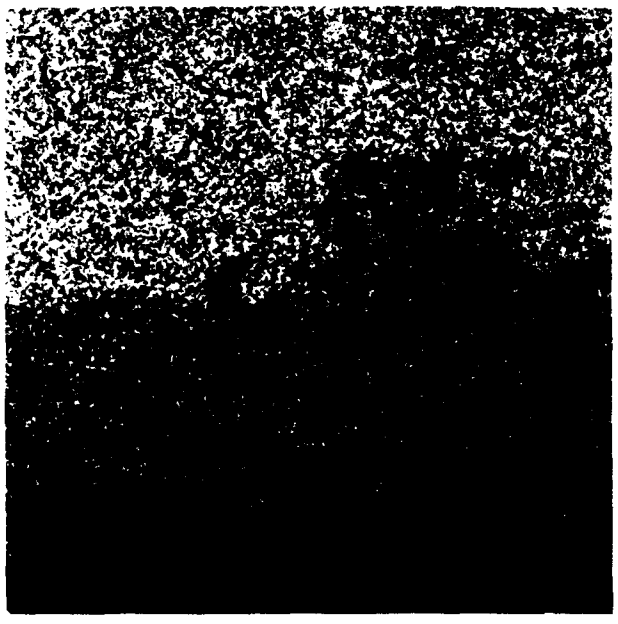

(a)

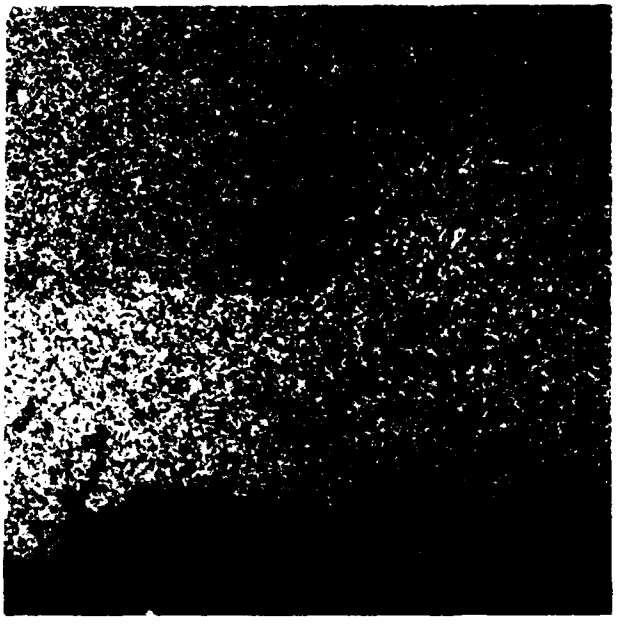

(b)

Figure 23. Micrographs and EDS maps of $MoSi_2$ heat treated in vacuum at 1650°C for 8 h: (a) Si map and (b) Mo map.

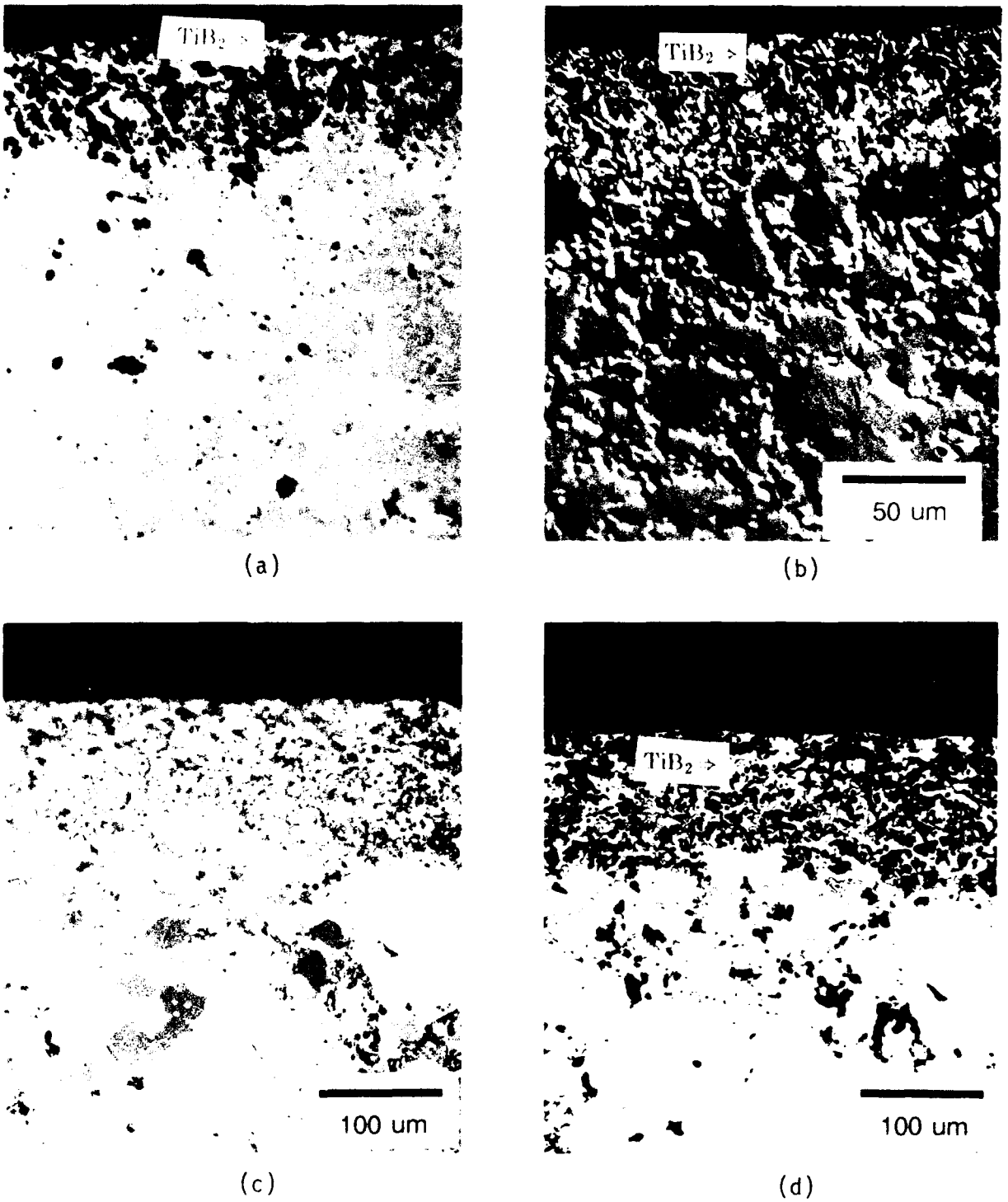

Figure 24. Micrographs of specimens of $MoSi_2$ + 20% TiB_2, heat treated in vacuum at 1650°C for (a) 2 h (Polarized), (b) 2 h (Nomarski), (c) 8 h (Polarized), and (d) 8 h (Nomarski).

Table 4 - Comparison of Thickness of Scales Formed on the Surface of the Composite $MoSi_2$ + 20% TiB_2 and Monolithic $MoSi_2$.

In air at 1650°C

Time	Composite	$MoSi_2$
15 min	1.7μm	.4μm
1 hour	4.2μm	1.0μm
4 hour	18 μm	2.5μm

In vacuum at 1650°C

Time	Composite	$MoSi_2$
2 hour	34μm (max. 62 μm)	18μm (max. 29 μm)
8 hour	95μm (max. 125 μm)	86μm (max. 105μm)

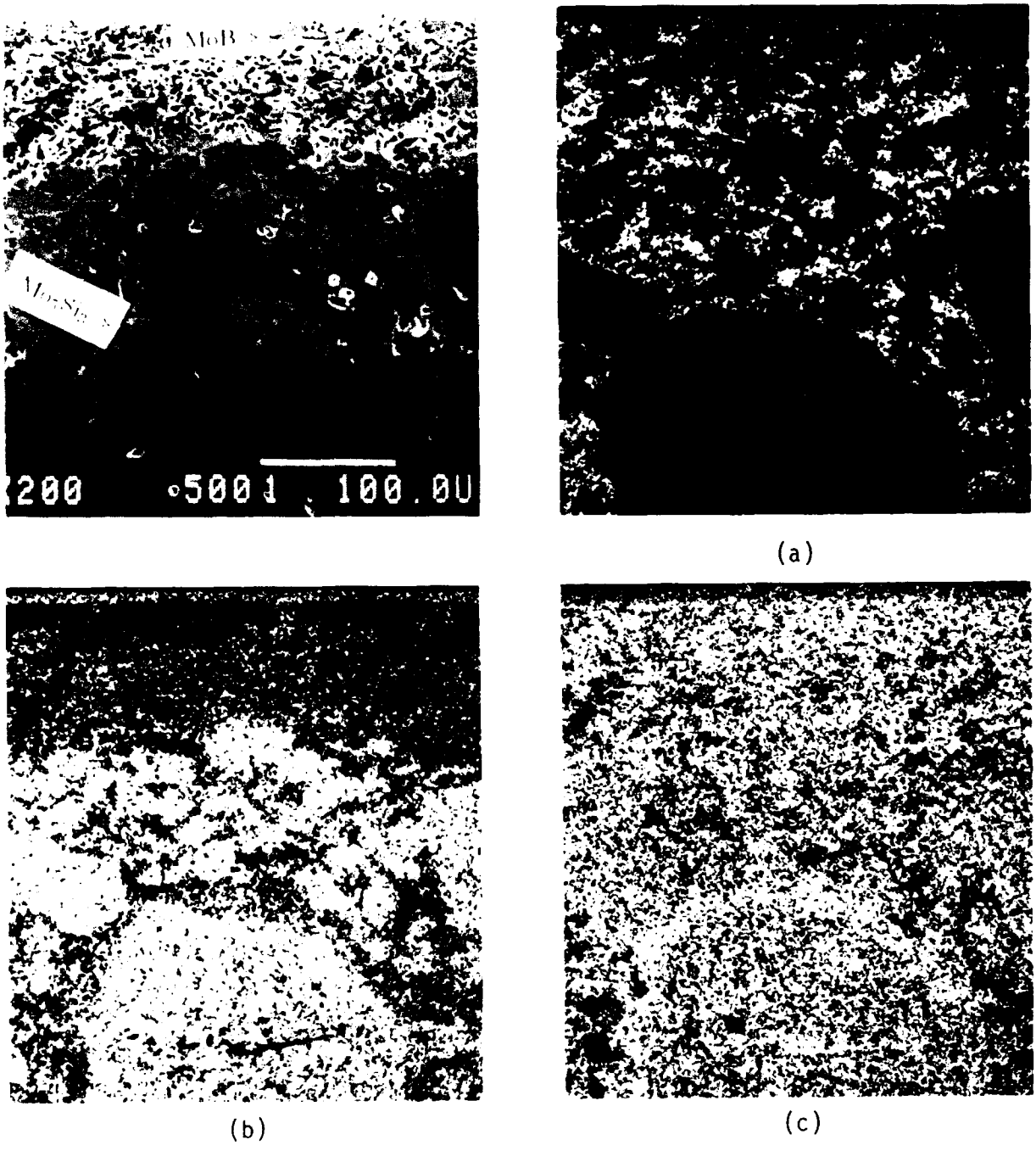

(a)

(b)

(c)

Figure 25. Micrographs and EDS maps of $MoSi_2$ + 20% TiB_2 heat treated in vacuum at 1650°C for 8 h: (a) Ti map, (b) Si map and (c) Mo map

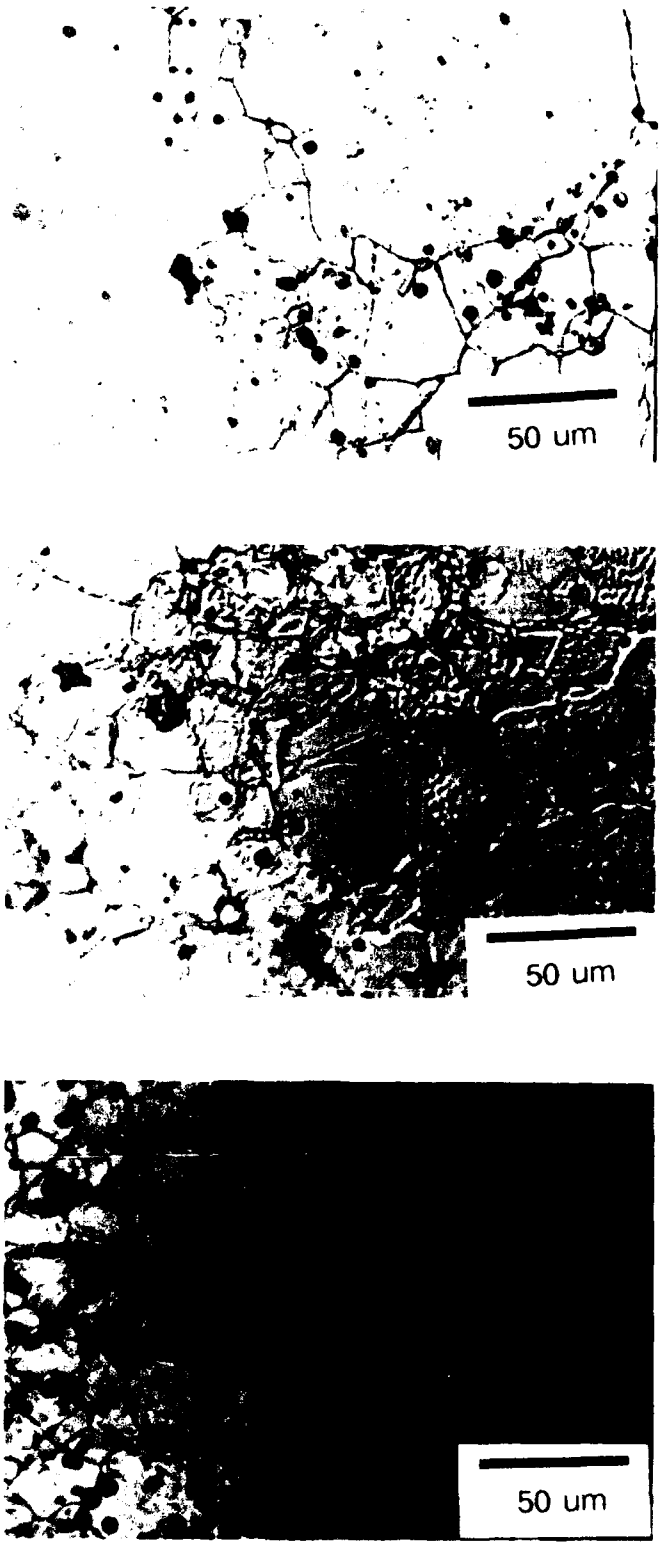

Figure 26. Micrographs of surfaces of $MoSi_2$ specimens heat treated in air for 1650°C for (a) 15 min, (b) 1 h and (c) 4 h

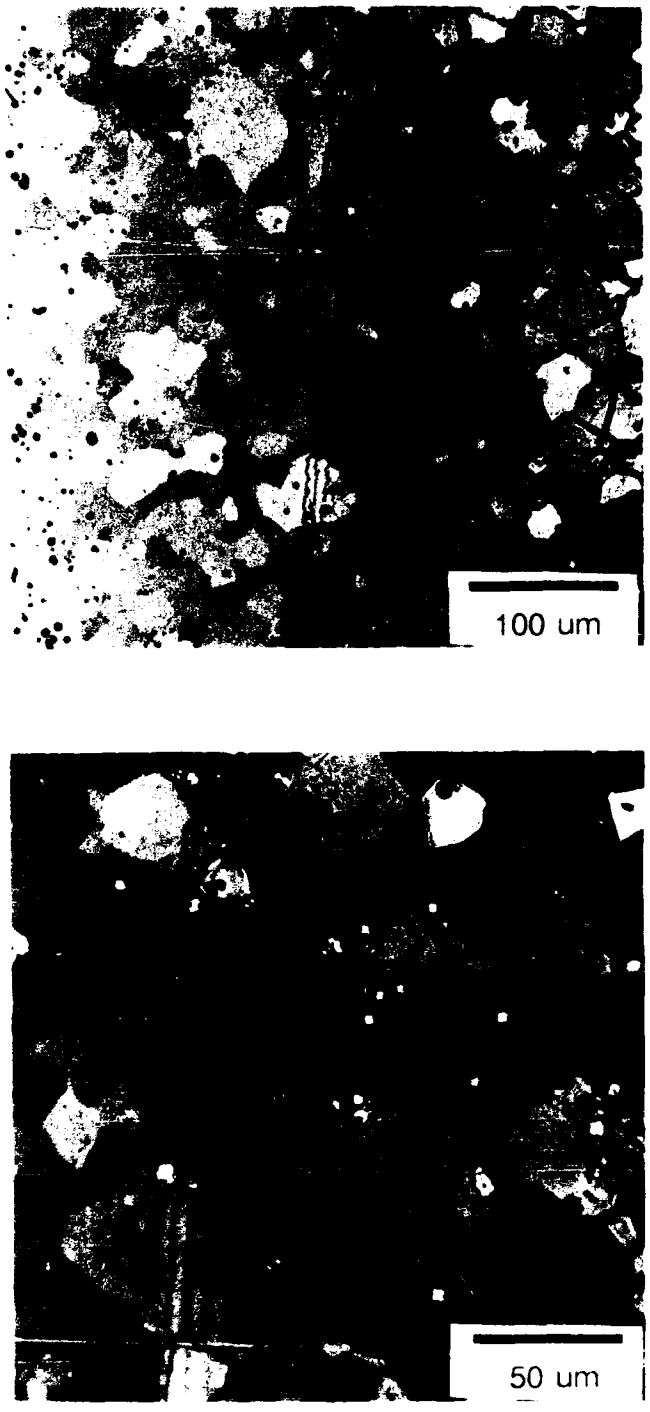

Figure 27. Micrographs of surface of $MoSi_2$ specimens heat treated in air at 1650°C for 4 h and polished at an angle of about 10°.

intermediate layer of Mo_5Si_3 does not form. A micrograph of the cross section of a sample exposed for 4 h in air at 1650°C as illustrated in Figure 28 and confirms the presence of a glassy layer on the surface of the specimen without a Mo_5Si_3 layer under it. The reason for the absence of a layer of Mo_5Si_3 is not clear but it is possible that the oxidation of the $MoSi_2$ under the glassy layer is stoichiometric, in which case the whereabouts of the resulting Mo oxides is not known.

(ii) $MoSi_2$ + 20% TiB_2:

When the composite sample is exposed to air at 1650°C, a glassy protective layer is once again formed although the thickness of this layer is much larger than that on the monolithic $MoSi_2$ samples (Table 4). In addition, crystals of TiO_2 are observed within this glassy layer near the glass alloy interface, as illustrated in the surface micrographs (Figure 29) and the micrographs of the cross sections (Figure 30). The glassy layer is once again protective, but appears to be not as protective as the pure silica layer on the $MoSi_2$. This is believed to be because the layer in the case of the composite specimen consists of significant amounts of B_2O_3. Nevertheless, the presence of the glassy layer prevents any significant reaction of the diboride particle even near the surface of the composite compact. The glassy layer contains significant amounts of crystalline TiO_2 in addition to a borosilicate glass. It is interesting that in this case the glassy layer has a thin layer of Mo_5Si_3 underneath it (as illustrated in Figure 31), suggesting that the presence of B_2O_3 in the glass somehow modifies the oxidation of the $MoSi_2$ underneath to a nonstoichiometric type. The effect of B_2O_3 in making the silica less protective is not surprising since B_2O_3 lowers the melting point and, hence, the viscosity of the silica as illustrated in Figure 32.

5.3 SANDWICH COMPOSITES:

Since it appeared that in the particulate composites described above, reaction begins with the diboride particles very close to the surface of the composites, some sandwich composites i.e., composite

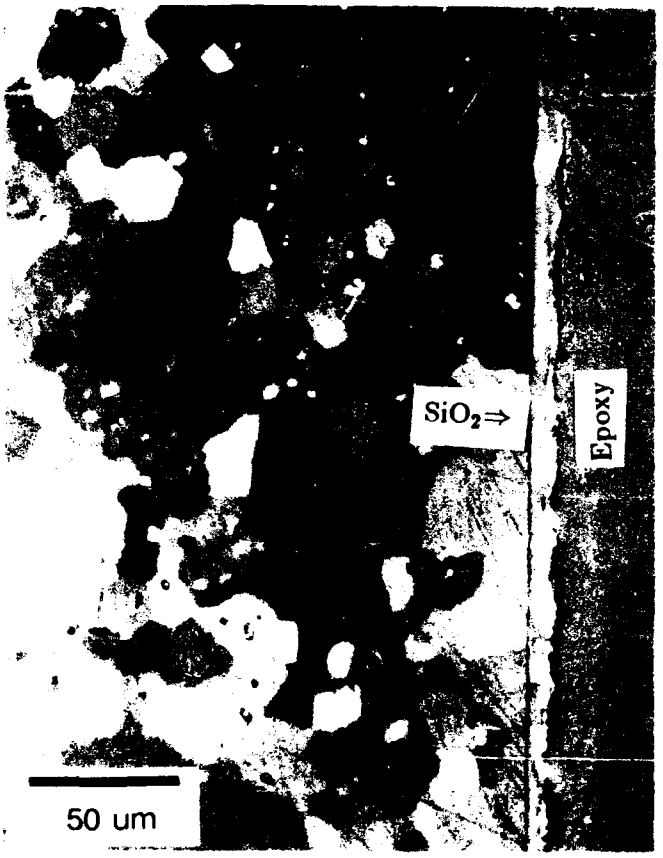

Figure 28. Micrograph of cross section of $MoSi_2$ specimens heat treated in air at 1650°C for 4 h.

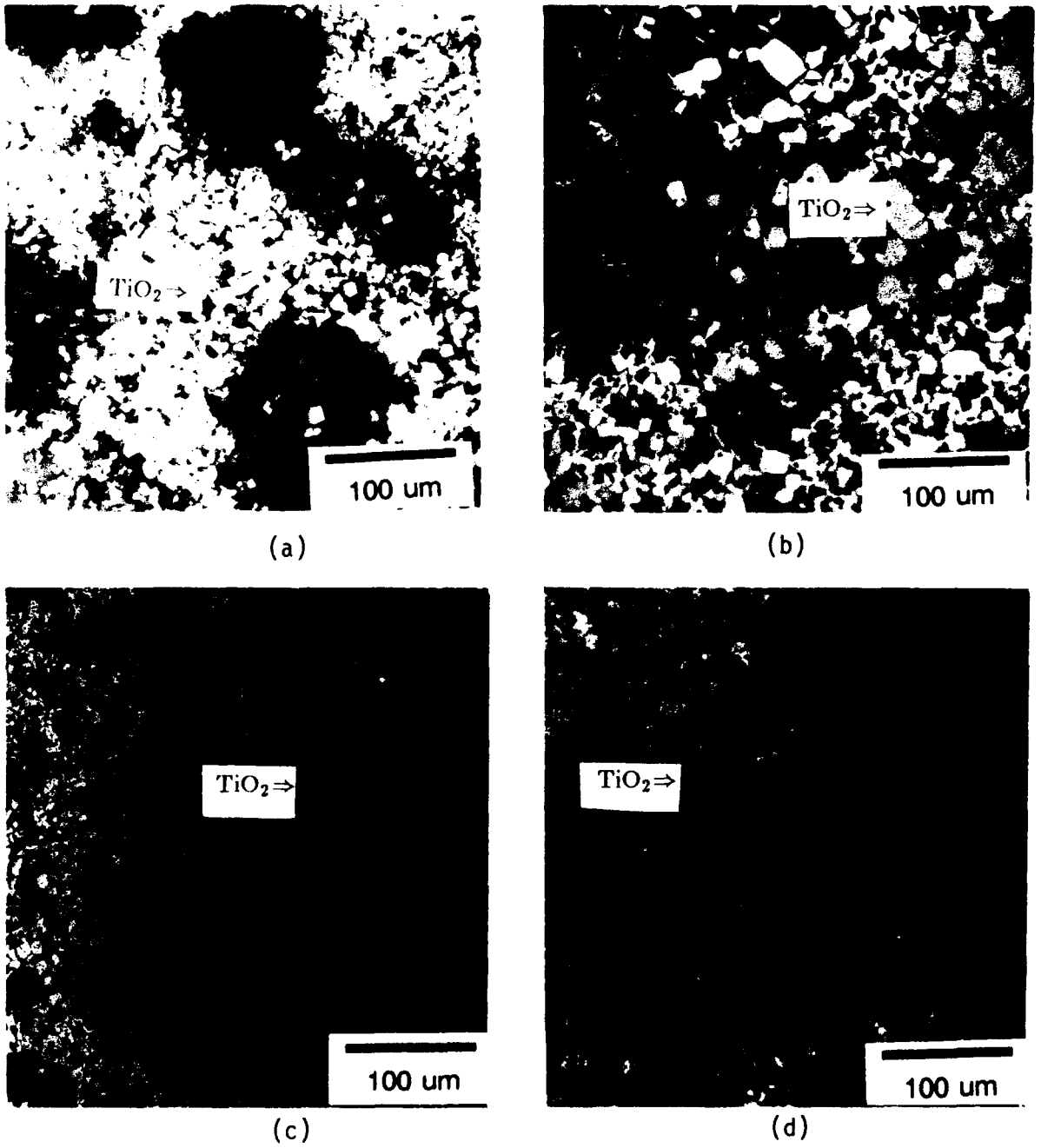

Figure 29. Micrographs of surfaces of $MoSi_2$ + 20% TiB_2 specimens heat treated in air at 1650°C for (a) 15 min, (b) 1 h and (c) 4 h.

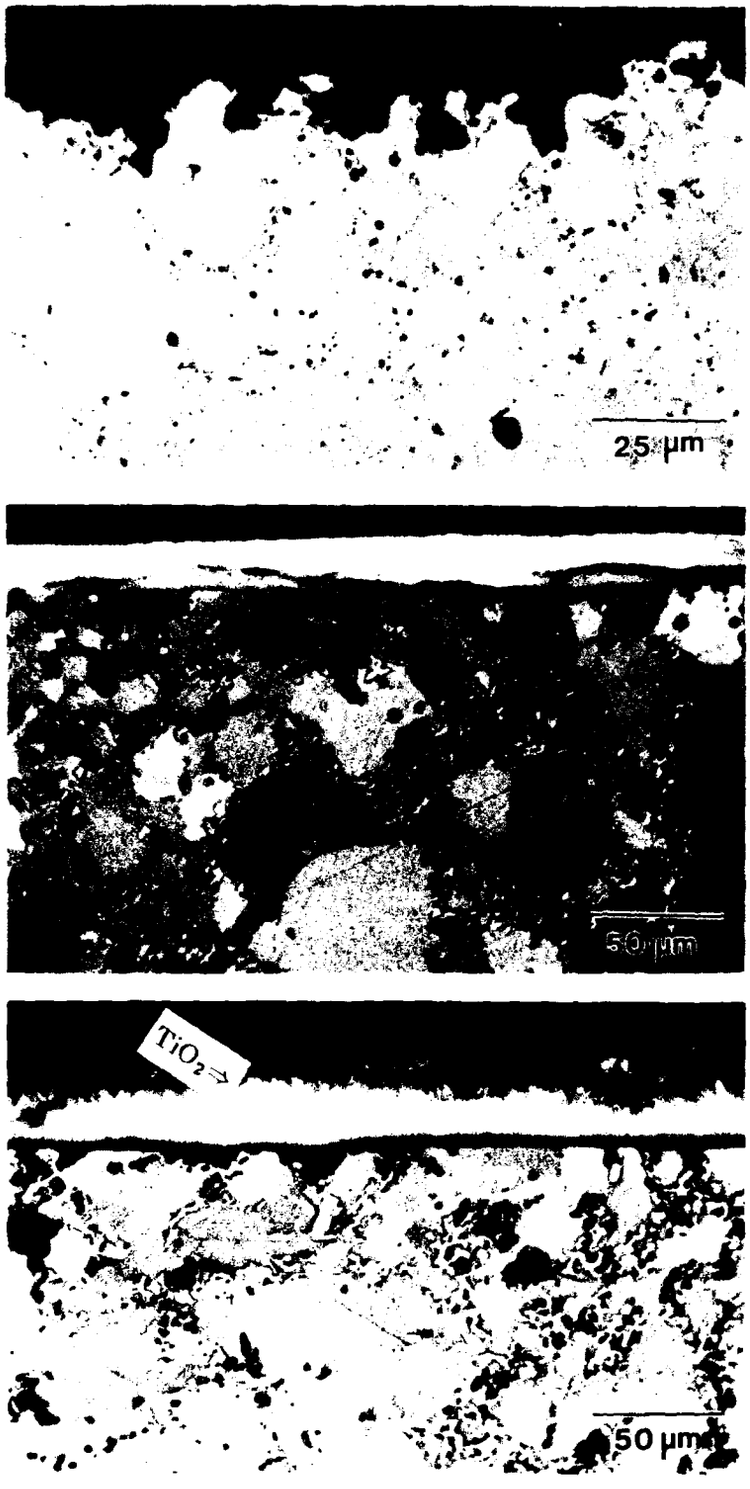

Figure 30. Micrographs of cross sections of $MoSi_2$ + 20% TiB_2 specimens heat treated in air at 1650°C for (a) 15 min, (b) 1 h and (c) 4 h.

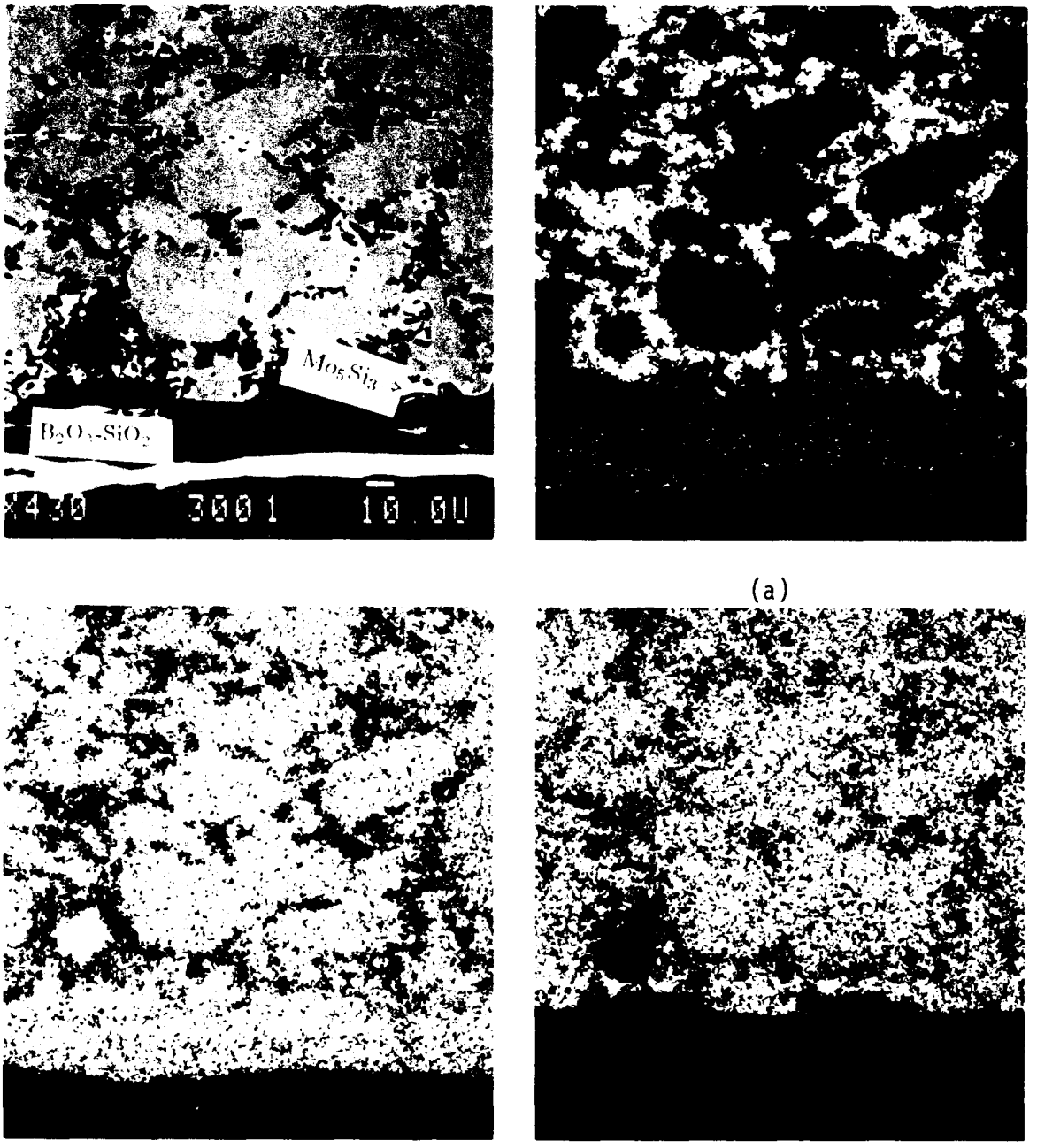

Figure 31. Micrographs and EDS maps of $MoSi_2$ + 20% TiB_2 heat treated in air at 1650°C for 4 h: (a) Ti map, (b) Si map and (c) Mo map.

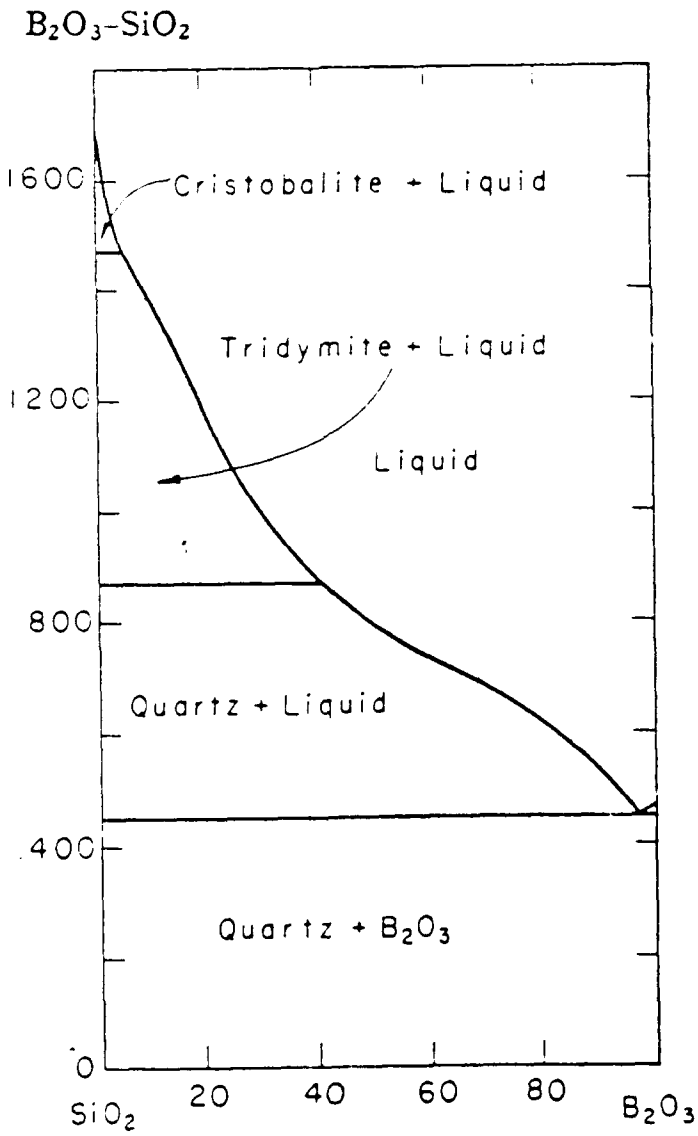

Figure 32. Phase diagram for SiO_2-B_2O_3.

compacts embedded in oxides matrices were prepared in order to evaluate the effectiveness of the matrices in preventing transport of oxygen. Such sandwich composites, although effective in slightly delaying the degradation of the diboride particles further inside the compact, were not very effective in reducing the degradation dramatically, suggesting that transport of oxygen through the oxides is very rapid and increasing the thickness of the oxide layer is not enough to slow the process significantly. The specimens of this type, when exposed to air at 1650°C, however, provide some understanding of the manner in which the B_2O_3 vapor makes its way out of the compact. The ZrO_2 grain boundaries are opened up for the escape of B_2O_3 for a sandwich composite of ZrO_2 + 5% TiB_2 inside ZrO_2.

Several attempts were made to modify the matrix with higher level of Y_2O_3 in the YS-ZrO_2, and were not much better than the results described above.

Since the disilicides were so effective in delaying the oxidation of the diborides, a sandwich composite was made. Monolithic diboride (2 mm x 2 mm x 2 mm) was hot pressed in $MoSi_2$ powder and samples of this were further hot pressed in Al_2O_3 powder. Specimens of this type were exposed to temperatures as high as 1800°C for extended periods of time and showed no significant reactions. These results point to the promise for using Al_2O_3 matrix composites with disilicides as oxidation barriers between the oxide matrix and diboride reinforcement. Figure 33 illustrates micrographs of the interfaces between the diboride and silicide, on one side, and that between the disilicide and the Al_2O_3 on the other side, for sandwich composite specimens exposed to 1650°C for 1 h and 1850°C for 1.5 h. An intermediate diffusion layer of Mo_5Si_3 is formed at the interface diffusion layer and the thickness of this zone increases with the temperature of exposure.

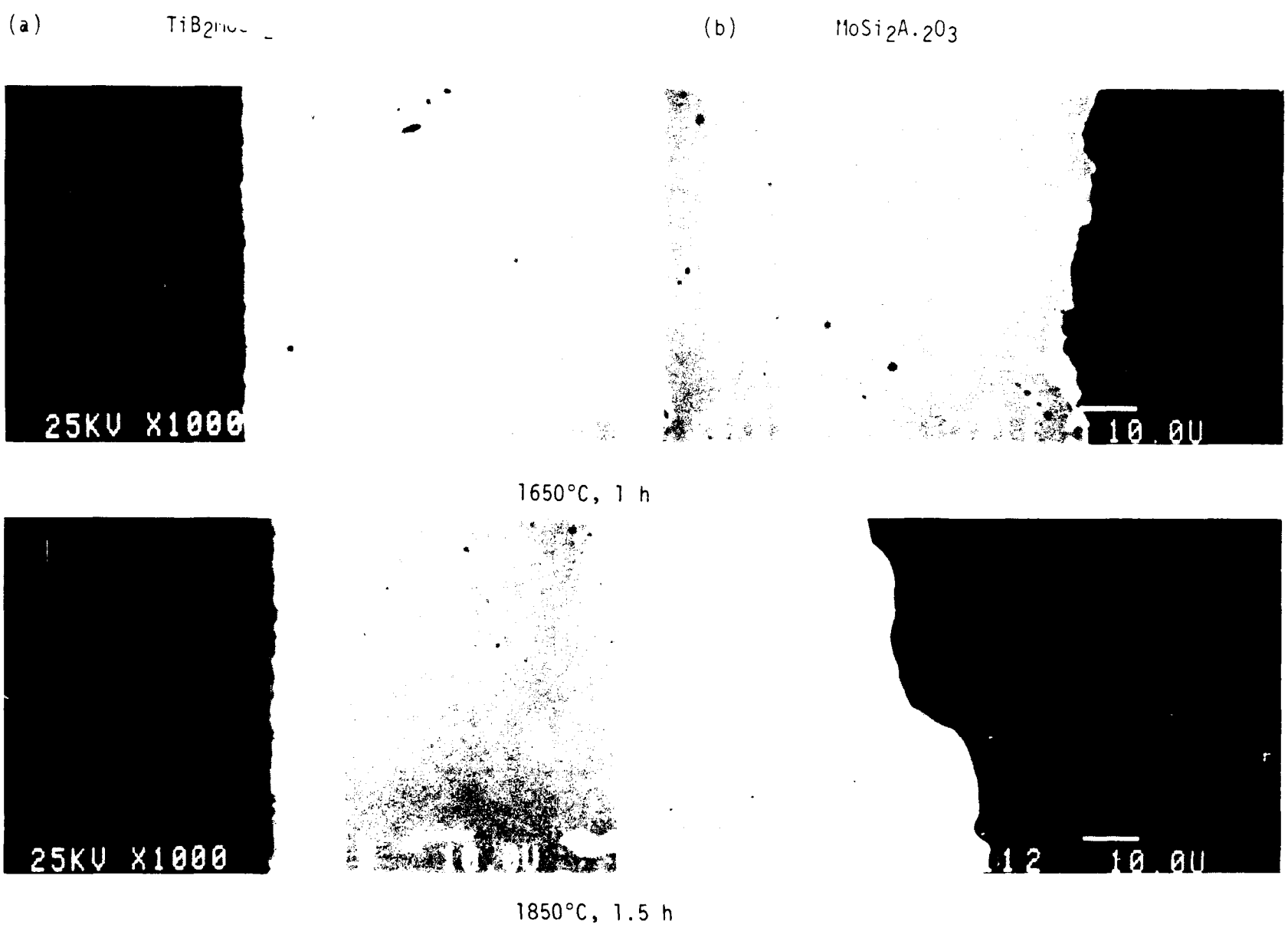

Figure 33. Sandwich composite of TiB_2MoSi_2/Al_2O_3 exposed to 1650°C, 1 h and 1850°C for 1.5h. (a) $TiB_2/MoSi_2$ interfaces and (b) $MoSi_2/Al_2O_3$ interfaces.

6. CONCLUSIONS AND RECOMMENDATIONS

The use of diborides as reinforcements in matrices of ZrO_2 and Y_2O_3 for very high temperature structural applications in oxidizing environments has serious limitations because of the rapid transport of oxygen through these oxides and consequent rapid oxidation of the diborides to B_2O_3 vapor. Even at temperatures of 1650°C, the diboride reinforcements oxidize completely in very short periods of time, and leave behind a porous sponge of the matrix oxides.

Although Al_2O_3 and $CaZrO_3$ with their tighter crystal structures are slightly better than the ZrO_2 and Y_2O_3 (which have open crystal structures), even these matrices allow rapid penetration of oxygen through them at ultrahigh temperatures. The oxygen penetrates to the interface of the diboride reinforcement and leads to the formation of liquid phase due to the interactions between several types of oxides including the very low-melting B_2O_3. Hence even at 1650°C, in short periods of exposure to air, even though pores are not formed, the diborides rapidly enter the liquid phase which forms an interconnected network.

The disilicides, on the other hand, offer a promising matrix for the diborides, since in air the Si forms a protective silica glass. The silica glass slows the transport of oxygen to the diboride particle to a considerable extent at 1650°C. However, the reaction of the diboride near the surface with the silica results in the formation of a more fluid and less protective borosilicate glass. In spite of this, the possibility of using silicides either as matrix materials or as barrier layers appears to be promising.

Further work needs to be carried out to evaluate these promising trends with disilicides for longer periods of exposure and to identify the details of the mechanisms involved. Some of these mechanistic discussions based on the present report will be published in graduate theses and technical papers which are being prepared.

Nevertheless, although the oxide matrix composites are not promising for applications in air, they behave very well at these temperatures in vacuum environments, since the combinations of oxides and diborides are found to be extremely compatible based on the observations of hot-pressed samples and samples exposed to vacuum.

REFERENCES

1. J.R.Ramberg and W.S.Williams, J. Mat. Sci., Vol. 22, p. 1815, 1987.

2. H.C.Graham, H.H.Davis, I.A.Kvernes and W.C.Tripp, USAF Contract F-33(615)-69-C-1017, 34-48.

3. R.J.Irving and I.G.Worsley, J. of Less Common Metals, Vol. 16, p. 103, 1968.

4. J.B.Berkowitz-Mattuck, J. Electrochem. Soc., Vol. 113, No. 9, p. 909, 1966.

5. W.C.Tripp and H.C.Graham, J. Electrochem. Soc., Vol. 118, No. 7, p. 1197, 1971.

6. A.K.Kuriakose and J.L.Margrove, J. Electrochem. Soc., Vol. 111, No. 17, p. 827, 1964.

7. W.C.Tripp, H.H.Davis and H.C.Graham, Ceramic Bulletin, Vol. 52, No. 8, p. 612, 1973.

8. T.E.Mitchell, A.H.Heuer, K.Vedula, Proceedings of the Ultra High Temperature Ceramic-Ceramic Composites Workshop, November 1986.

9. C.D.Wirkus and D.R.Wilder, "High Temperature Oxidation of Molybdenum Disilicides," J. Am. Ceram. Soc., 49(4), pp. 173-77, 1960

10. Y.A.Chang, "Oxidation of Molybdenum Disilicide," J. Mater. Sci., pp. 4641-43, 1969.

11. V.A.Lavrenko, V.Z.Shemet and A.V.Goncharuk, "Studies on Mechanism of High-Temperature Oxidation of Molybdenum, Tungsten, and Zirconium Sisilicides by Differential Thermal Analysis," Thermochimica Acta, pp. 501-04, 1986.

12. J.Berkowitz-Mattuck, "High Temperature Oxidation II. Molybdenum Silicides," J. Electrochem. Soc., 112(6) pp. 583-89, 1965.

13. E.A.Irene and Y.J.Van der Meulen, "Silicon Oxidation Studies: Analysis of SiO(g) Film Growth Data," J. Electrochem. soc., 123(9), 1380084, 1976.

14. B.E.Deal and A.S.Grove, "General Relationship for the Thermal Oxidation of Silicon," J. Appl. Phys., 30(12), pp. 3770-78, 1965.

15. M.A.Janney, "Mechanical Properties and Oxidation Behavior of a Hot-Pressed SiC-15-vol 5% TiB_2 Composite," Am. Ceram. Soc. Bull., 66(2), pp. 322-24, 1987.

16. JANAF Thermocheical Tables, 2nd ed., D.R.Stull and H.Prophet, Project Directors, Washington, U.S. National Bureau of Standards, U.S. Printing Printing Office, 1971.

17. K.Vedula, A.Abada, W.Williams, Proceedings of the MRS Symposium, Spring 1988 (in press).

U.S. Government Printing Office 548-076